FINAL REPORT TR-559
IMPROVED METHOD FOR DETERMINING WIND LOADS ON HIGHWAY SIGN AND TRAFFIC-SIGNAL STRUCTURES

By George Constantinescu, Asghar Bhatti and Talia Tokyay

Submitted to

Iowa Highway Research Board
800 Lincoln Way, Ames, Iowa 50010

The University of Iowa
Department of Civil and Environmental
Engineering &
IIHR-Hydroscience and Engineering
Hydraulics Laboratory
Iowa City, IA 52242-1585
Phone: 319-335-5237

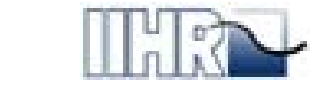

About the IIHR- Hydroscience & Engineering

IIHR, a unit of The University of Iowa's College of Engineering, is one of the nation's premier and oldest fluids research and engineering laboratories. Situated on the Iowa River in Iowa City, Iowa, IIHR seeks to educate students and to conduct research in the broad fields of hydraulics and fluid mechanics.

Disclaimer Notice

The contents of this report reflect the views of the authors, who are responsible for the facts and the accuracy of the information presented herein. The opinions, findings and conclusions expressed in this publication are those of the authors and not necessarily those of the sponsors. The sponsors assume no liability for the contents or use of the information contained in this document. This report does not constitute a standard, specification, or regulation. The sponsors do not endorse products or manufacturers. Trademarks or manufacturers' names appear in this report only because they are considered essential to the objective of the document.

Non-discrimination Statement

The University of Iowa does not discriminate on the basis of race, color, age, religion, national origin, sexual orientation, gender identity, sex, marital status, disability, or status as a U.S. veteran. Inquiries can be directed to the Director of Equal Opportunity and Diversity at the University of Iowa, (319) 335-0705.

IMPROVED METHOD FOR DETERMINING WIND LOADS ON HIGHWAY SIGN AND TRAFFIC-SIGNAL STRUCTURES

Final report

December 2007

Principal Investigators

Dr. George Constantinescu and Dr. Asghar Bhatti
IIHR - Hydroscience & Engineering and
Civil and Environmental Engineering
The University of Iowa
Iowa City, IA 52242

Research Assistant

Talia Tokyay
IIHR-Hydroscience & Engineering
The University of Iowa
Iowa City, Iowa 52242

Sponsored by
Iowa Highway Research Board (IHRB Project TR-559)

A report from
IIHR-Hydroscience & Engineering
College of Engineering
The University of Iowa
Iowa City, Iowa 52242
Phone: 319-335-5237
Fax: 319-335-5238
www.iihr.uiowa.edu

Technical Report Documentation Page

<table>
<tr><td>Report No.
TR-559</td><td colspan="2">2. Government Accession No.</td><td>3. Recipient’s Catalog No.</td></tr>
<tr><td colspan="2" rowspan="2">4. Title and Subtitle
Improved Method for Determining Wind Load on Highway Sign and Traffic Signal Structures</td><td colspan="2">5. Report Date
December 2007</td></tr>
<tr><td colspan="2">6. Performing Organization Code</td></tr>
<tr><td colspan="2">7. Author(s)
George Constantinescu, Asghar Bhatti, Talia Tokyay</td><td colspan="2">8. Performing Organization Report No.</td></tr>
<tr><td colspan="2" rowspan="2">9. Performing Organization Name and Address
The University of Iowa
Department of Civil and Environmental Engineering &
IIHR-Hydroscience and Engineering
Hydraulics Laboratory
Iowa City, IA 52242-1585</td><td colspan="2">10. Work Unit No. (TRAIS)</td></tr>
<tr><td colspan="2">11. Contract or Grant No.</td></tr>
<tr><td colspan="2" rowspan="2">12. Sponsoring Organization Name and
Iowa Highway Research Board
Iowa Department of Transportation
800 Lincoln Way
Ames, IA 50010</td><td colspan="2">13. Type of Report and Period Covered
Final Report</td></tr>
<tr><td colspan="2">14. Sponsoring Agency Code</td></tr>
<tr><td colspan="4">15. Supplementary Notes</td></tr>
<tr><td colspan="4">16. Abstract
The main objective of the proposed study is to use Computational Fluid Dynamics (CFD) tools to determine the wind loads by accurate numerical simulations of air flow characteristics around large highway sign structures under severe wind speeds conditions. Fully three-dimensional Reynolds-Averaged Navier-Stokes (RANS) simulations are used to estimate the total force on different panels, as well as the actual pressure distribution on the front and back faces of the panels. In particular, the present study investigates the effects of aspect ratio and sign spacing for regular panels, the effect of sign depth for the dynamic message signs that are now being used on Iowa highways, the effect induced by the presence of back-to-back signs, the effect of the presence of add-on exit signs, and the effect of the presence of trucks underneath the signs potentially creating “wind tunnel” effect.</td></tr>
<tr><td colspan="3">17. Key Words
wind load, highway signs, RANS</td><td>18. Distribution Statement
No restrictions.</td></tr>
<tr><td>19. Security Classification (of this report)
Unclassified.</td><td>20. Security Classification (of this page)
Unclassified.</td><td>21. No. of Pages
79</td><td>22. Price
NA</td></tr>
</table>

Table of Contents

	Section	Page Number
	List of Figures	v
	List of Tables	ix
	Acknowledgement	x
	Abstract	xi
1.	Problem Statement and Background	1
2.	Description of Test Cases and Objectives	4
3.	Numerical Model	7
4.	Discussion of Results	12
	a. Investigation of effects of aspect ratio and sign spacing for regular panels	14
	b. Investigation of the effect of sign depth for dynamic message signs	19
	c. Investigation of the effect induced by the presence of back-to-back signs	19
	d. Investigation of the effect of the presence of add-on exit Signs	23
	e. Investigation of the effect due to the passage of trucks	23
	f. Investigation of the effect of air holes in a rectangular panel	25
5.	Conclusions and Recommendations for Future Work	27
6.	References	30
7.	Appendix	31

List of Figures

Name of the Figure — Page Number

Figure 1: Damage to two highway structures due to high winds…… 32

Figure 2. Sketch showing possible disposition patterns for the holes on the panel and main geometrical parameters…….. 32

Figure 3. General views of the computational domain and mesh for case 1……... 33

Figure 4. General view of the mesh; a) in a plane perpendicular to the flow, b) in a plane parallel to the bottom of the domain, c) in a plane parallel to the sides of the domain.. 33

Figure 5. Pressure (left), streamwise velocity (middle) and TKE (right) distributions in a vertical plane cutting through the symmetry axis of the panel in case 1…… 34

Figure 6. Pressure (left), streamwise velocity (middle) and TKE (right) distributions in a horizontal plane cutting through the symmetry axis of the panel in case 1…… 34

Figure 7. Distributions on the back side pressure (top), the front side pressure (middle) and the pressure difference between the two sides (bottom) for case 1. The dimensional pressure levels (psf) are shown. …… 35

Figure 8. Distributions on the back side pressure (top), the front side pressure (middle) and the pressure difference between the two sides (bottom) for the panels considered in case 2. The dimensional pressure levels (psf) are shown…….. 36

Figure 9. Distributions on the back side pressure (top), the front side pressure (middle) and the pressure difference between the two sides (bottom) for the panels considered in case 3. The dimensional pressure levels (psf) are shown…….. 37

Figure 10. Distributions on the back side pressure (top), the front side pressure (middle) and the pressure difference between the two sides (bottom) for the panels considered in case 4. The dimensional pressure levels (psf) are shown. …… 38

Figure 11. Distributions on the back side pressure (top), the front side pressure (middle) and the pressure difference between the two sides (bottom) for the panels considered in case 5. The dimensional pressure levels (psf) are shown…….. 39

Figure 12. Distributions on the back side pressure (top), the front side pressure (middle) and the pressure difference between the two sides (bottom) for the panels considered in case 6. The dimensional pressure levels (psf) are shown…….. 40

Figure 13. Distributions on the back side pressure (top), the front side pressure (middle) and the pressure difference between the two sides (bottom) for the panels considered in case 7. The dimensional pressure levels (psf) are shown…….. 41
Figure 14. Distributions on the back side pressure (top), the front side pressure (middle) and the pressure difference between the two sides (bottom) for the dynamic message sign considered in case 8. The dimensional pressure levels (psf) are shown. …….. 42
Figure 15. Distributions on the back side pressure (top), the front side pressure (middle) and the pressure difference between the two sides (bottom) for the thin panel considered in case 9. The dimensional pressure levels (psf) are shown…… 43
Figure 16. Visualization of the solution for case 10 in a horizontal plane cutting at mid-height level through the center of the panels; a) non-dimensional pressure contours, b) TKE contours, c) streamlines…….. 44
Figure 17. Distributions on the back side pressure (top), the front side pressure (middle) and the pressure difference between the two sides (bottom) for the panels considered in case 10. The dimensional pressure levels (psf) are shown. The relative position of the two panels is shown in the sketch……. 45
Figure 18. Visualization of the solution for case 11 in a horizontal plane cutting at mid-height level through the center of the panels; a) non-dimensional pressure contours, b) TKE contours, c) streamlines…….. 46
Figure 19. Distributions on the back side pressure (top), the front side pressure (middle) and the pressure difference between the two sides (bottom) for the panels considered in case 11. The dimensional pressure levels (psf) are shown. The relative position of the two panels is shown in the sketch……. 47
Figure 20. Visualization of the solution for case 12 in a horizontal plane cutting at mid-height level through the center of the panels; a) non-dimensional pressure contours, b) TKE contours, c) streamlines…….. 48
Figure 21. Distributions on the back side pressure (top), the front side pressure (middle) and the pressure difference between the two sides (bottom) for the panels considered in case 12. The dimensional pressure levels (psf) are shown. The relative position of the two panels is shown in the sketch. ……... 49

Figure 22. Visualization of the solution for case 13 in a horizontal plane cutting at mid-height level through the center of the panels; a) non-dimensional pressure contours, b) TKE contours, c) streamlines…….. 50
Figure 23. Distributions on the back side pressure (top), the front side pressure (middle) and the pressure difference between the two sides (bottom) for the panels considered in case 13. The dimensional pressure levels (psf) are shown. The relative position of the two panels is shown in the sketch……. 51
Figure 24. Distributions on the back side pressure (top), the front side pressure (middle) and the pressure difference between the two sides (bottom) for the panel considered in case 14. The dimensional pressure levels (psf) are shown……. 52
Figure 25. Distributions on the back side pressure (top), the front side pressure (middle) and the pressure difference between the two sides (bottom) for the panel with an add-on sign considered in case 15. The dimensional pressure levels (psf) are shown. Figure 26. The relative position of the panel and the two trucks in case 16……... 53
Figure 26. The relative position of the panel and the two trucks in case 16…… 54
Figure 27. Distributions on the back side pressure (left) and the front side pressure (right) for the panel and the two trucks considered in case 16. The dimensional pressure levels (psf) are shown. The relative position of the panel and the two trucks is indicated in the figure…….. 55
Figure 28. Visualization of the numerical solution for case 16 in a vertical plane cutting through the middle of one of the trucks. a) pressure contours; b) streamwise velocity contours; c) 2D streamline patterns; d) TKE contours…… 56
Figure 29. Visualization of the numerical solution for case 16 in a horizontal plane cutting through the middle of the panel sign. a) pressure contours; b) streamwise velocity contours; c) 2D streamline patterns; d) TKE contours…….. 57
Figure 30. Visualization of the computational mesh for panel with holes in a spanwise plane. a) the mesh on the panel and around it, b) detail near one of the holes showing the transition from the hole region to the surrounding domain……... 58
Figure 31. Visualization of the computational mesh for the panel with holes in a vertical plane cutting through the middle of the panel. a) general view, b) detail view of the mesh near the panel……. 59

Figure 32. Streamlines in a vertical plane passing through the center of the panel. a) panel without holes, b) panel with holes, c) detail view, panel without holes, d) detail view, panel with holes……. 60
Figure 33. Pressure contours in a vertical plane passing through the center of the panel. a) panel without holes, b) panel with holes, c) detail view, panel without holes, d) detail view, panel with holes…….. 61
Figure 34. Streamwise velocity contours in a vertical plane passing through the center of the panel. a) panel without holes, b) panel with holes, c) detail view, panel without holes, d) detail view, panel with holes…… 62
Figure 35. Turbulent kinetic energy (TKE) contours in a vertical plane passing through the center of the panel. a) panel without holes, b) panel with holes, c) detail view, panel without holes, d) detail view, panel with holes……. 63
Figure 36. Streamlines in a horizontal plane passing through the center of the panel. a) panel without holes, b) panel with holes, c) detail view, panel without holes, d) detail view, panel with holes…… 64
Figure 37. Pressure contours in a horizontal plane passing through the center of the panel. a) panel without holes, b) panel with holes, c) detail view, panel without holes, d) detail view, panel with holes……... 65
Figure 38. Streamwise velocity contours in a horizontal plane passing through the center of the panel. a) panel without holes, b) panel with holes, c) detail view, panel without holes, d) detail view, panel with holes…… 66
Figure 39. Turbulent kinetic energy contours in a plane passing through the center of the panel. a) panel without holes, b) panel with holes, c) detail view, panel without holes, d) detail view, panel with holes…….. 67

List of Tables

Name of the Table Page Number

Table 1. Geometrical characteristics of the simulations containing panels without holes……. 6

Table 2. Summary of the pressure forces and wind loads on the various panels for the 16 cases……. 13

Acknowledgement

We would like to thank the Technical Advisory Committee (TAC) for the Iowa DOT members, Mr. Ahmad Abu-Hawash, Mr. Dean Bierwagen and Mr. Kenneth Dunken for their contributions to this work.

.

Abstract

Accurate estimation of wind forces on large highway sign structures is important due to possible structural failure of these sign structures under strong winds. The panels of these structures are becoming large and increasingly more common as we attempt to better manage the highway traffic flow and automate the highway systems. In recent years, there is increasing evidence that design of such structures does not take into account the specific loadings experienced by these large panel structures. Consequently, some of these structures have required frequent inspections, retrofitting, and even premature replacement. In order to be able to predict behavior of these structures accurate knowledge of the forces on these structures must to be known.

An important aspect of wind loads on highway structures that is generally not appreciated is the effect of interactions among the panel structures on these forces. The main objective of the proposed study is to use Computational Fluid Dynamics (CFD) tools to determine the wind loads by accurate numerical simulations of air flow characteristics around large highway sign structures under severe wind speeds conditions. Fully three-dimensional Reynolds-Averaged Navier-Stokes (RANS) simulations are used to estimate the total force on different panels, as well as the actual pressure distribution on the front and back faces of the panels. The pressure distributions are needed in case a detailed structural dynamics analysis will be performed.

In particular, the present study investigates the effects of aspect ratio and sign spacing for regular panels, the effect of sign depth for the dynamic message signs that are now being used on Iowa highways, the effect induced by the presence of back-to-back signs, the effect of the presence of add-on exit signs, and the effect of the presence of trucks underneath the signs potentially creating “wind tunnel” effect. The reduction in the mean pressure force on the panels as a result of the presence of small air holes in a wide rectangular panel is also investigated. Recommendations for future work are provided.

1. Problem Statement and Background

Highway structures such as signals, signposts and luminaries are susceptible to wind-induced loads that include flutter, buffeting, vortex-shedding, and wind-rain/ice vibrations. Accurate estimation of wind forces especially on large highway sign structures is important due to possible structural failure of these sign and traffic signal structures under strong wind conditions. The panels of these structures are becoming large and there are more of these structures as we attempt to better manage the highway traffic flow and to automate the highway systems. In recent years, there is increasing evidence that the specific loadings that these large panel structures are subjected to are not accounted for properly during their design. Consequently, there have been recent cases of collapse of these structures due to high winds (see Figure 1). In some cases, the highway structures had to be removed prematurely because they were not meeting the performance criteria.

The standard code-based design of highway structures considers static wind loads based on the expected maximum wind speeds. The AASHTO *Standard Specifications for Structural Supports for Highway Signs, Luminaires and Traffic Signals* (2001 and 2003 interim specifications) have been recently revised through a major research project conducted under the auspices of the National Cooperative Highway Research Program (NCHRP 17-10). The 2003 document includes updated provisions and criteria for extreme wind loads and new provisions and criteria on fatigue design. However, the methods used to obtain the new provisions and criteria in the AASHTO Standard are still essentially based on a static strength design approach. The structures designed in this manner may have adequate factor of safety against strength failure but their response to aeroelastic phenomena is largely unknown. For example, flutter may cause torsional vibrations that usually receive little consideration in design. Buffeting may cause large structural motions and over time can induce fatigue damage. An additional phenomenon that is often overlooked in the design of these structures is the effect of unsteady oscillations on the panels and on the traffic signal supports. These oscillations develop even under steady wind conditions mainly due to the unsteady vortex shedding which takes place in the air wake of the flow past the panels of the highway signs and traffic signals.

After a highway structure is built the occurrence of any one of the aforementioned wind related effects would require countermeasures that could be quite expensive. Thus, it is necessary to account for these phenomena as early in the design/construction cycle as possible. A basic prerequisite is to have a rational understanding of these effects and to develop appropriate procedures and tools that can be used efficiently in the design process.

Additionally, there is a need to determine how best to minimize wind loads on structure supporting signs and lights. Several options are available for doing this:

- Develop improved shape and dimensions of signs and their support structures
- Develop air-flow panels (panels with holes disposed on a certain pattern) to reduce wind loadings (especially drag form) and addition of flow-modifying fixtures.

Most of the current guidelines for wind design of highway structures are based on wind tunnel studies with some limited field investigations. The wind tunnel studies provide valuable insight but, besides being expensive, they have obvious limitations because of the differences in the laboratory and field conditions and limited amount of data that can be collected in such studies. In the past there was essentially no other alternative. However recent advances in the computational fluid dynamics (CFD) have made tools available that allow realistic simulations of actual field conditions at a fraction of the cost of wind tunnel studies. Additionally, with three-dimensional (3D) simulations, it is possible to visualize the entire 3D airfields and the associated pressure and shear stress distributions on the structures. Also, CFD allows investigating in a quantitative way the interactions among the panels in the case of structures supporting multiple traffic signs.

It is also important to note that wind tunnel testing will not provide the necessary insight needed to develop the design improvements. In mechanical engineering and civil engineering, it has been realized that resort must be made to Computational Fluid Dynamics (CFD) modeling together with computational structural dynamics techniques, to obtain advanced insights that would facilitate estimation of aerodynamic and hydrodynamic loads. The output from CFD solvers can be easily used with computational structural dynamics techniques to test a particular design under a certain set of wind conditions (e.g., direction, magnitude, etc.).

In this exploratory project we used state-of-the-art CFD computational tools to study the wind loads on highway structures. At the start of the project it was decided to focus in this exploratory study on the estimation of wind loads (total forces and their distributions on the panel surface) on typical Iowa highway structures. To accomplish this it was decided to carry out RANS simulations and include multiple sign panels with various aspect ratios. Furthermore it was decided that there is no need to consider holes in the panels (an idea that was part of the original proposal) because the current DOT practice does not include holes in the highway signs because of readability concerns. Rather the study focused on multiple sign panels with various aspect ratios. Iowa DOT is especially interested in larger signs which allow better readability (larger lettering). As a result of the discussions a matrix of cases to be simulated was developed.

Among the research topics of interest to Iowa DOT the present study tries to provide at least preliminary answers to the following questions:

- What are the wind pressure distributions on rectangular signs?
- What is the effect of rectangular sign aspect ratio on the wind pressure and its distribution?
- How are the pressure distributions on rectangular signs with small rectangular add-on signs different from the pressure distributions on signs without add-on signs?
- What is the effect of absolute size of rectangular signs on the wind pressures?
- What is the effect on wind pressure distribution of several adjacent signs resulting in slot-shaped holes between them?
- What is the effect on wind pressures when signs are shielded by other signs on the "back side" side of the sign truss?
- What is the effect of the depth of the signs on the wind pressure distributions?

Additionally, the present set of simulations will serve to better understand the range of conditions over which the empirical formula used to determine the mean pressure difference between the two sides of a panel is adequate. The formula used by Iowa DOT for signs placed on cantilevered or overhead trusses is:

$$\Delta P = K_z G V I_r C_d \qquad (1)$$

where

K_z = height and exposure factor (~1.0)
G = gust effect factor (~1.14)
V = design wind velocity (generally 90 mph)
I_f = importance factor (=1)
C_d = drag coefficient (~1.2-1.27)

For a design wind velocity of 90 mph (~50 m/s), the pressure difference calculated using this empirical formula is in the rage of 28 to 30 psf. Thus, for the various cases studied, a central question is whether or not the estimate of 30 psf is conservative enough.

2. Description of Test Cases and Objectives

The final list approved by the TAC for this preliminary "proof-of-concept" phase of the project consists of a total of 16 cases. The complete list summarizing the main geometrical dimensions of the panels and their relative position is given in Table 1. In all cases the wind direction is perpendicular to the panels, corresponding to the case when the maximum wind load is expected to occur on the panels.

Results from these simulations will allow better understanding of:

- the effects of aspect ratio and sign spacing for regular panels (7 simulations),
- the effect of sign depth for the dynamic message signs that are now being used on Iowa highways (2 simulations),
- the effect induced by the presence of back-to-back signs (4 simulations),
- the effect of the presence of add-on exit signs (2 simulations).
- the effect due to the passage of trucks. The last case considers a sign situated at a finite distance from the road level with two trucks obstructing the airflow beneath it.

The height of the panel was used to non-dimensionalize the results in the CFD simulations. The non-dimensional velocity is the velocity of the incoming wind speed (90 mph). This makes the physical Reynolds number to be around 7.5 million.

We also investigated the effects of the presence of air holes in a rectangular panel (aspect ratio 1:2) with two arrays of small holes (the holes area represents 2.5% of the total panel surface) disposed in a collocated arrangement (see Figure 2), and the associated reduction in the total force acting on the panel.

The main objectives of this study are to obtain information on the airflow around highway sign and traffic signal structures and then to estimate the wind loads (forces) acting on them using state-of-the-art CFD tools. In this proof-of-concept study we concentrate on aspects of direct interest to Iowa DOT. For each case, the total force and the average pressure on the different panels, as well as the actual pressure distribution on the front and back faces of the panels, are calculated. Especially, for the cases where multiple panels are situated side by side or on two parallel rows at a relatively small distance, CFD allows a much more accurate quantification of these forces. As a result of the proximity between the panels the pressure forces on the panels may be considerably different from those calculated by considering each panel independently using CFD or empirical formulae. The pressure distributions are needed in case a detailed structural dynamics analysis will be performed in the future.

The main outcome of this study will be a better understanding of the effects of wind on highway sign and traffic signal structures. The results of the present study can be used to better understand the accuracy of the empirical formulae typically used in the design process by Iowa DOT (e.g., to estimate forces on panels of a certain size).

Table 1. Geometrical characteristics of the simulations containing panels without holes.

Cases	Height (ft)	Width (ft)	Thickness (ft)	Number of Plates	Distance between Plates (ft)	Position of the Plates
1	14.75	55	-	1	-	-
2	14.75	W1 = 27 W2 = 27	-	2	1	Side by side
3	14.75	W1 = 24 W2 = 24	-	2	7	Side by side
4	14.75	W1 = 24 W2 = 12	-	2	12	Side by side
5	14.75	W1 = 12 W2 = 12 W3 = 12	-	3	9.5	Side by side
6	12	70	-	1	-	-
7	12	W1 = 24 W2 = 24	-	2	22	Side by side
8	10.17	W = 32	6.42	1		-
9	10.17	W = 32	-	1	-	-
10	14.75	W1 = 24 W2 = 24	-	2	d_b =6.67	Back to back
11	14.75	W1 = 24 W2 = 24	-	2	d_b = 6.67 d_s = 12	Back to back Side by side
12	14.75	W1 = 24 W2 = 24	-	2	d_b = 6.67 d_s = 24	Back to back Side by side
13	14.75	W1 = 24 W2 = 24	-	2	d_b = 6.67 d_s = 30	Back to back Side by side
14	8.5	22.5	-	1	-	-
15	H = 8.5 h = 2.5	W1 = 22.5 W2 = 9	-	2	-	Small on top of large one
16	H =10.17 ht1 = ht2 = 11.5	W = 32 wt1 = wt2 = 8.5	T = 6.42 tt1 = tt2 = 6.42	1	Distance between the trucks and the plate = 4	Trucks under the plate

3. Numerical Method

Most predictions of engineering flows are obtained using the so-called Reynolds Averaged Navier-Stokes (RANS) approach in which the effect of most of the scales (eddies, vortices) on the mean flow is accounted via a RANS turbulence model.

RANS based numerical simulations were performed using Fluent, a commercial Computational Fluid Dynamics (CFD) general software for modeling fluid flow and heat transfer in complex geometries. As a preprocessor for geometry modeling and mesh generation, Gambit® was used. Gambit allows the user to generate high quality meshes using unstructured multi-block grids. Fluent can use a wide range of turbulence models with both wall functions and near-wall treatment to simulate turbulent flows.

The parallel pressure based RANS solver was employed to conduct steady-state simulations. The implicit RANS solver employs a cell centered finite volume scheme and can use hybrid unstructured meshes. The continuity equation is satisfied using the SIMPLE pressure-velocity algorithm. Gradients of the solution variables are computed using Green-Gauss' theorem. Diffusion terms are discretized using second order central scheme. For the convective terms, there are several choices offered in the code including first order upwind, second order upwind, QUICK and third order MUSCL schemes. For the convective terms in the momentum equations, the second order upwind scheme was chosen as the discretization scheme in the present simulations. The discretized equations are solved using point wise Gauss-Seidel iteration in conjunction with an algebraic multi-grid method to accelerate the solution convergence.

The shear stress transport (SST) model which can be integrated up to the wall was used as the turbulence model. A full description of the model is given in Fluent User's Guide (2001). The SST version uses the classical k-ω model (k is the turbulence kinetic energy, ω is the specific turbulence dissipation rate) near solid walls and the high Reynolds number version of the k-ε model away from the solid walls and inside the free-shear layers. Major features are the zonal weighting of the model coefficients and limiting the eddy viscosity growth in rapidly strained flows. The switching between the k-ω and k-ε models is achieved using blending functions for

the values of the model coefficients. To blend the k-ω and k-ε models, the latter is rewritten using a transformation of variables into a k-ω like form. As a result of the transformation of variables, an additional cross-diffusion term appears in the ω equation corresponding to the k-ε model. The k-ω SST model allows simple Dirichlet boundary conditions to be specified at the wall for the transported turbulence quantities.

The SST model has a performance very similar to that of the original k-ω model, but without the undesirable free-stream dependency. The new model was found to lead to improvements in the prediction of adverse pressure gradient flows. Several studies have shown that SST is one of the most accurate RANS models in predicting complex vortical flows like the ones considered in the present study where massive flow separation occurs as the airflow is convected past the panels.

The SST model is similar to the standard k-ω model for which the equations are given as:

$$\frac{\partial}{\partial t}(\rho k) + \frac{\partial}{\partial x_i}(\rho k u_i) = \frac{\partial}{\partial x_j}(\Gamma_k \frac{\partial k}{\partial x_j}) + G_k - Y_k \tag{2}$$

$$\frac{\partial}{\partial t}(\rho \omega) + \frac{\partial}{\partial x_i}(\rho \omega u_i) = \frac{\partial}{\partial x_j}(\Gamma_\omega \frac{\partial \omega}{\partial x_j}) + G_\omega - Y_\omega + D_\omega \tag{3}$$

In these equations ρ is the density, k is the turbulent kinetic energy, u_i is the velocity component in the i direction, t is the time and ω is the specific dissipation rate. G_k represents the generation of turbulent kinetic energy due to mean velocity gradients. G_ω represents the generation of ω. Γ_k and Γ_ω represent the effective diffusivity of k and ω, respectively. Y_k and Y_ω are the dissipation of k and ω due to the turbulence. D_ω represents the cross diffusion term.

The effective diffusivity for the SST model is given by:

$$\Gamma_k = \mu + \frac{\mu_t}{\sigma_k} \tag{4}$$

$$\Gamma_w = \mu + \frac{\mu_t}{\sigma_\omega} \tag{5}$$

where μ is the molecular viscosity of the flow and μ_t is the turbulent viscosity. σ_k and σ_w are the turbulent Prandtl numbers for k and ω, respectively. The turbulent viscosity μ_t is computed as follows:

$$\mu_t = \frac{\rho k}{\omega} \frac{1}{\max\left[\frac{1}{\alpha^*}, \frac{\Omega F_2}{a_1 \omega}\right]} \tag{6}$$

where Ω may be computed as

$$\Omega \equiv \sqrt{2\Omega_{ij}\Omega_{ij}} \tag{7}$$

The expressions for the model coefficients are:

$$\sigma_w = \frac{1}{F_1 / \sigma_{\omega,1} + (1 - F_1) / \sigma_{\omega,2}} \tag{8}$$

$$\sigma_k = \frac{1}{F_1 / \sigma_{k,1} + (1 - F_1) / \sigma_{k,2}} \tag{9}$$

where Ω_{ij} is the mean rate of rotation tensor and the coefficient α^* is introduced to damp the turbulent viscosity and it acts as a low-Reynolds number correction. It is given by:

$$\alpha^* = \alpha^*_\infty \left(\frac{\alpha^*_0 + \mathrm{Re}_t / R_k}{1 + \mathrm{Re}_t / R_k} \right) \tag{10}$$

where

$$\mathrm{Re}_t = \frac{\rho k}{\mu \omega}, R_k = 6, \alpha^*_0 = \frac{\beta_i}{3}, \beta_i = 0.072.$$

For the high Reynolds-number version of the SST model, α^* and α_∞^* are assumed to be one. The blending functions F_1 and F_2 are given by

$$F_1 = \tanh(\phi_1^4) \tag{11}$$

$$\phi_1^4 = \min\left[\max\left(\frac{\sqrt{k}}{0.09\omega y}, \frac{500\mu}{\rho y^2 \omega}\right), \frac{4\rho k}{\sigma_{\omega,2} D_\omega^+ y^2}\right] \tag{12}$$

$$D_\omega^+ = \max\left[2\rho \frac{1}{\sigma_{\omega,2}} \frac{1}{\omega} \frac{\partial k}{\partial x_j} \frac{\partial \omega}{\partial x_j}, 10^{-20}\right] \tag{13}$$

$$F_2 = \tanh(\phi_2^2) \tag{14}$$

$$\phi_2^2 = \max\left(2\frac{\sqrt{k}}{0.09\omega y}, \frac{500\mu}{\rho y^2 \omega}\right) \tag{15}$$

The blending function F_2 served to modify the formulation of the eddy viscosity inside the boundary layers, such that the k-ω SST model can better account for the transport of the turbulent stresses. Its expression depends on the wall distance, *y*. This leads to significantly improved predictions of separated flows by avoiding common problems observed with the standard k-ω model (e.g., under-prediction of the separation caused by adverse pressure gradients).

The term G_k represents the production of turbulent kinetic energy, and is defined similarly as in the standard k-ω model.

$$G_k = \mu_t S^2 \tag{16}$$

where S is the magnitude of the rate of strain tensor. The term G_ω represents the production of ω and is given by

$$G_\omega = \frac{\alpha}{\nu_t} G_k \tag{17}$$

Note that this formulation differs from the standard k-ω model. Another difference between the k-ω and SST models is in the way the term α_∞ is evaluated. In the standard k-ω model α_∞ is defined as a constant, $\alpha_\infty = 0.52$. In the SST model, α_∞ is given by

$$\alpha_\infty = F_1 \alpha_{\infty,1} + (1 - F_1)\alpha_{\infty,2} \tag{18}$$

$$\alpha_{\infty,1} = \frac{\beta_{i,1}}{\beta^*_\infty} - \frac{\kappa^2}{\sigma_{\omega,1}\sqrt{\beta^*_\infty}} \tag{19}$$

$$\alpha_{\infty,2} = \frac{\beta_{i,2}}{\beta^*_\infty} - \frac{\kappa^2}{\sigma_{\omega,2}\sqrt{\beta^*_\infty}} \tag{20}$$

where κ is 0.41 and $\beta_{i,1}$ and $\beta_{i,2}$ are 0.075 and 0.0828 respectively. The term Y_k represents the dissipation of turbulence kinetic energy.

$$Y_k = \rho\beta^* k\omega \tag{21}$$

The term Y_ω represents the dissipation of ω.

$$Y_\omega = \rho\beta_i \omega^2 \tag{22}$$

Instead of having a constant value, β_i is given by

$$\beta_i = F_1 \beta_{i,1} + (1 - F_1)\beta_{i,2} \tag{23}$$

where $\beta_{i,1}$ and $\beta_{i,2}$ are 0.075 and 0.0828 respectively. To blend the k-ε and k-ω models together, the standard k-ε model equations have been transformed into equations based on k and

ω, which leads to the introduction of a cross-diffusion term (D_ω). In the SST formulation D_ω is defined as

$$D_\omega = 2(1-F_1)\rho\sigma_{\omega,2}\frac{1}{\omega}\frac{\partial k}{\partial x_j}\frac{\partial \omega}{\partial x_j} \tag{24}$$

The other model constants are:

$$\sigma_{k,1} = 1.176 \quad \sigma_{\omega,1} = 2.0$$
$$\sigma_{k,2} = 1.0 \quad \sigma_{\omega,2} = 1.168 \tag{25}$$
$$a_1 = 0.31 \quad \beta_{i,1} = 0.075 \quad \beta_{i,2} = 0.0828$$

A mass outflow boundary was used in the exit section in all simulations. The lateral boundaries were placed at a large distance from the panel and symmetry boundary conditions were used. The panel surfaces were treated as a no slip surface. The flow in the streamwise direction was uniform in the inflow section that was placed at a considerable distance upstream of the panels.

4. Discussion of Results

Tables 1 and 2 summarize the main geometrical characteristics of the 16 simulations discussed in sections 4a to 4e, the non-dimensional and dimensional (psf) mean pressure difference of each of the panels and the total wind load on each of the panels. For each simulation the pressure distributions over the two faces of the panel are also provided. In all the cases the height of the main panels is 14.75 ft and the wind speed is 90 mph which matches the design wind velocity in Iowa for these kinds of panels. The wind direction is perpendicular to the panels.

Table 2. Summary of the pressure forces and wind loads on the various panels for the 16 cases.

		Average Pressure Force Non-dimensional		$\Delta F = F_{back} - F_{front}$	$\Delta F = F_{back} - F_{front}$	$\Delta P = P_{ave}^{back} - P_{ave}^{front}$	$\Delta P = P_{ave}^{back} - P_{ave}^{front}$
Cases	**Position**	**Front**	**Back**	**Non-dimensional**	**Pound-force**	**Non-Dimensional**	**Psf**
1		-0.436	-3.044	2.607	23,948	0.699	29.52
2	Right	0.831	-0.557	1.388	12,764	0.759	32.05
	Left	0.831	-0.557	1.388	12,764	0.759	32.05
3	Right	1.010	-0.098	1.108	10,188	0.680	28.78
	Left	1.010	-0.102	1.112	10,188	0.682	28.78
4	Large	-0.3587	0.7045	1.0632	9,770	0.652	27.60
	Small	-0.2229	0.3483	0.5712	5,266	0.705	29.75
5	Right	-0.2686	0.3048	0.5734	5,287	0.7079	29.87
	Middle	-0.2590	0.3070	0.5660	5,222	0.6988	29.50
	Left	-0.2680	0.3048	0.5728	5,287	0.7072	29.87
6		0.4030	3.0980	2.6950	21,658	0.7005	29.58
7	Right	0.9910	0.0795	0.9115	7,325	0.6904	29.16
	Left	0.9910	0.0795	0.9115	7,325	0.6904	29.16
8		1.0712	0.2074	0.8638	6,942	0.5769	23.88
9		1.0826	0.13	0.9526	7,655	0.6362	26.87
10	Front	1.4480	0.1348	1.3132	10,554	0.8056	34.02
	Back	0.1164	0.5163	-0.3999	-3,214	-0.2453	-10.36
11	Front	1.2320	-0.0010	1.2330	9,909	0.7565	31.95
	Back	0.5722	0.1906	0.3816	3,067	0.2341	9.89
12	Front	0.7253	-0.5942	1.3195	10,604	0.8095	34.20
	Back	0.6896	-0.2937	0.9833	7,902	0.6033	25.49
13	Front	1.4171	0.1122	1.3049	10,487	0.8006	33.83
	Back	1.4171	0.2761	1.1410	9,170	0.7000	29.58
14		0.5835	-0.0271	0.6106	4907	0.6881	28.49
15	Small	0.0600	-0.0144	0.0744	598	0.7175	30.32
	Large	0.6030	-0.0703	0.6733	5411	0.7587	32.06
16		0.8443	0.2496	0.8904	8020	0.5947	24.64

4.a Investigation of effects of aspect ratio and sign spacing for regular panels

A general view of the computational domain used for Case 1 simulation (one panel) is shown in Figure 3. As indicated in Table 1, the panel size was 14.75 ft by 55 ft. The thickness of the panel is only 0.06 in. This is the largest size panel normally used for highway signs. The panel was considered to be situated away from the ground and the incoming wind speed at the level of the panel to be approximately constant.

The size of the domain surrounding the panel was around 15H in the vertical and spanwise directions. The total length of the domain in the streamwise direction was around 75H. These dimensions are representative for all the 15 simulations. In the last simulations, the bottom boundary was a no-slip wall corresponding to the road. The panels were considered as no-slip surfaces on which all the velocity components were set equal to zero. Around 1.5 million grid points were used to generate the mesh. The first grid points off the wall surfaces were situated at less than 100 wall units from the panel.

The distributions of the pressure, streamwise velocity and the Turbulent Kinetic Energy (TKE) in a vertical plane and in a horizontal plane cutting through the symmetry axes of the panel are shown in Figures 5 and 6, respectively. The pressure values are high on the upstream face of the panel due to the fact that the incoming flow strongly decelerates (e.g., see distribution of the streamwise velocity in the same figures) as it approaches the panel. On the back of the panel the pressure distribution is not exactly uniform but the pressure levels inside the recirculation region behind the panel are much lower compared to the ones observed upstream of the panel. In the wake, the pressure recovers slowly as one moves downstream while the streamwise velocity deficit is diminishing. The TKE is strongly amplified in the detached shear layers forming due to the separation of the boundary layer on the four sides of the panel. The other region where the TKE is strongly amplified is situated just behind the panel. Compared to the distributions of the pressure and the streamwise velocity the TKE decays much faster toward the levels associated with the free flow away from the panel region. These characteristics of the flow around the panel are common to practically all of the cases of panels without holes considered in this study.

Thus, the following analysis of the various solutions will concentrate on the pressure distributions on the two faces of the panels that determine the total wind load.

As observed from Figure 7b, on the front side of the panel the largest pressure values (~20 psf) are observed to occur in a horizontal band in the central part of the panel. The extent of the horizontal band is determined by the aspect ratio of the panel which is large (close to 1:4). The pressure decreases as one moves toward the four edges of the panel. This is expected (Bernoulli law), as close to the edges the velocity is high as the flow moving toward the panel is diverted laterally and passes the panel. On the back of the panel (Figure 7a) the largest levels are also observed in the central part of the panel (~ -10 psf). However, the distribution is different than the one observed on the front side of the panel. The pressure on the back side of the panel decreases much faster as one moves toward the edges. As a result, the relative pressure distribution in Figure 4c has two regions of high values situated close to the two extremities of the panel in the horizontal direction. In this region the effective pressure is above 32 psf. Still, even in the central region of the panel the values of ΔP are still around 25 psf. The values are very small near the edges because the pressure field is continuous and the panel is thin. The mean (integrated) value of the pressure difference on the panel is 29.52 psf. This corresponds to a wind load of about 23.95 pound-force. The nondimensional values are also indicated in Table 2. The wind load is proportional with the surface of the panel. However, the value of the mean pressure difference is expected to be much less dependent on the size and shape of the panel, at least for isolated panels or for panels that do not interact with each others.

Case 1 is a case for which one expects the design formula used by Iowa DOT should give good results, as only one isolated panel is considered. Indeed, as shown in Table 2 the estimated value of the mean pressure difference between the two sides of the panel is 29.52 psf (non-dimensional value $\Delta P/\rho U^2=0.699$) which is very close to the rounded value of 30 psf obtained from the empirical formula.

The next case in the series (case 2) considers two panels of same size (width = 27 ft, height = 14.75 ft as for the panel in case 1) with a slot of 1 ft between them. The sum of the widths of the two panels and of the slot is identical to the width of the panel considered in case 1. The

presence of the slot allows the air to flow at high speeds in between the panels and reduces locally the pressure differences between the front and sides of the two panels close to the slot. This is again a consequence of the fact that the pressure and velocity fields are continuous. In a way, the slot plays the role of the air holes that are considered in section 4.f.

The flow is symmetrical with respect to the vertical (streamwise oriented) plane passing through the middle of the slot. Thus, the pressure distributions on the two panels are also symmetrical with respect to the same plane. The pressure distributions on the front face of the two panels (Figure 8b) show the largest pressure levels are obtained very close to the two edges on the sides of the slot openings. Compared to case 1, the region of relatively high pressure values on the front face is thicker in the vertical direction. On the back faces (Figure 8a), the largest pressures are observed at around 4 ft from the slot opening. The presence of the slot has a much larger influence on the pressure distributions on the back face of the panels (compare pressure distributions in Figure 7a and Figure 6a). As a result of the front and back distributions, the distribution of the effective pressure (Figure 8c) shows the largest values (~39 psf) are present very close to the vertical edge on the side of the slot opening where the pressure on the front peaks while the pressure on the back side is relatively small. A second area where the values of ΔP are relatively high (~33psf) is observed at 5-7 ft from the vertical edge opposite the slot. The reason is that the pressure on the front face is still relatively high while the pressure on the back side has decreased to the lowest levels on the panel surface.

When integrated, the mean pressure difference is 32.05 psf on both panels ($\Delta P/\rho U^2 = 0.759$). This value is slightly higher than the one observed in case 1. Though the simulation results clearly show the pressure distributions on the two panels are affected by their proximity, the average is comparable to empirical wind load formula. The total wind load on each panel is 12,764 pound-force (see Table 2).

In case 3, the slot opening is larger (7 ft) but the total width (two panels plus the slot opening) is the same (55 ft). Each panel has a width of 24 ft. The pressure distribution on the front of the two panels shown in Figure 9b is similar to the one observed in case 2. The only difference is that the maximum levels are situated at a larger distance from the vertical edge of the panel on

the slot side (see also Figure 8b). The same observation holds for the pressure distributions on the back side of the two panels (Figure 9a) in which the maximum pressure levels are situated practically at the center of the two panels rather than close to the vertical edge on the slot side (see Figure 8a corresponding to case 2). Though the distribution of the pressure difference still shows the presence of two regions of relatively high values, similar to case 2, the largest values are observed in the region situated close to the vertical edge situated on the outer flow side. Also, the overall pressure distribution on the two panels is more uniform compared to case 2.

The mean pressure difference on the two panels is 28.78 psf which is slightly lower than the one predicted for case 2 (32.05 psf) and case 1 (29.52). The wind load on each panel is 10,188 pound-force.

In case 4 the widths of the two panels (24 ft and 12 ft, respectively) are not anymore equal and the width of the slot is much larger 12 ft such that there is not much interaction between the two panels. This can be observed from the pressure distributions on the front (Figure 10b) and especially on the backs (Figure 10a) of the two panels that are relatively symmetric with respect to the center of each channel.

The mean pressure difference on the larger panel is 27.6 psf. The corresponding value for the smaller panel is 29.75. The difference is mainly explained by the different aspect ratio of the two panels rather by the way the airflow between the two panels influences the pressure distributions on the panels. The wind load on the larger panel is 9,770 pound-force. The wind load on the smaller panel is 5,266 pound-force.

In case 5, three identical panels with an aspect ratio close to one (height 14.75 ft, width 12 ft) are present. The width of the slot opening between two panels is large (9.5 ft) such that there is very little interaction between the panels. As a result, the pressure distributions on the front and back sides (Figures 11a and 11b) are very similar, both qualitatively and quantitatively, for the three panels. In fact, due also to the aspect ratio of the panels which is close to 1:1, the region of relatively high pressure values is close to circular. Similar to case 4, the pressure distributions on the front face of the panels appear to be more dependent on the presence of other panels.

The mean pressure difference on the three panels is 29.7 psf. The wind load on the panels is around 5,200 pound-force. These values are practically identical to those predicted in case 4 for the smaller panel (identical to the panels in case 5). This again proves that for relatively large width of the slot between the panels, the mean pressure difference and the wind load is practically independent of the presence of other (identical or larger) panels.

Case 6 investigates the effect of the aspect ratio for a large isolated panel. In this sense case 6 is directly comparable to case 1. The aspect ratio is close to 3.5 for case 1 and close to 5.3 for case 2. Qualitatively, the pressure distributions on the two faces of the panel are very similar in case 1 and case 6 (compare Figures 7 and 12). On the front side of the panel the pressure is relatively uniform until about 2 ft from the edges of the panel. On the back side the region of large pressure values is more elliptical and small values are observed to occur near the lateral extremities of the panel. This also explains the distribution of the pressure difference on the panel in cases 1 and 6. In fact, the mean pressure difference in cases 1 and 6 is practically identical (29.58 vs. 29.52 psf). The differences in the wind load (23,948 vs. 21,658) are due only to the different areas of the two panels in cases 1 and 6. Analysis of cases 1, 5, and 6 shows that the mean pressure difference is sensitive to the aspect ratio of the panel for relatively small values of this parameter (1:1 to 1:3). However, for values of the aspect ratio in the range 1:3 to 1:6 the mean pressure difference is practically independent of this parameter.

Case 7 investigates the effect of the aspect ratio for the panels of smaller height (12 ft). In this case two identical panels of width equal to 24 ft are positioned such that the width of the slot opening between them is 22 ft. Due to the large size of the slot opening one does not expect any strong interaction between the panels. The aspect ratio of the small panels is 1:2 which is close to the one in case 2. However, in case 2 there was a strong interaction among the two panels because the slot opening was relatively small (1 ft). In this regard case 3 is a much better case to compare with, even though the aspect ratio was closer to 1:1.7. The front and back pressure distributions in case 7 (Figure 13) are practically symmetrical with respect to the symmetry axes of the two panels which confirms there is very little interaction between the two panels. The mean pressure difference on the two panels is 29.16 psf which is very close to the one observed

in case 3 (28.78) and about 10% smaller than the one predicted in case 2 (32.05). The wind load on each panel is around 7,300 pound-force.

4.b Investigation of the effect of sign depth for dynamic message signs

The simulations in cases 8 and 9 consider the effect of sign depth on the pressure distributions. The panel has same dimensions in both simulations (32 ft wide and 10.17 ft high). In case 8 the depth of the panel is 6.42 ft corresponding to a typical dynamic message sign used on highways in the state of Iowa. In case 9 the same panel has a negligible thickness.

The pressure distributions on the front and back sides of the two panels are qualitatively similar in both simulations. In fact they also look similar to the other cases in which only one panel with a relatively high aspect ratio was considered (e.g., case 1).

The mean pressure difference on the thick panel is 24.06 psf. The corresponding value for the thin panel is 26.87 psf which means that thicker panels are in fact subjected to a slightly lower wind load if the surface of the panel and the wind velocity are the same.

4.c Investigation of the effect induced by the presence of back-to-back signs

In this section we consider the interaction between two rectangular signs of equal size (height is 14.75 ft, width is 24 ft similar to the panels considered in case 3). The two panels are situated in two parallel planes. The distance between the two planes is 6.67 ft. The changes in the pressure distributions on the panels are investigated as the relative position of the two panels changes from being back-to-back (case 10, Figure 16), to one panel being half-width behind the other (case 11, Figure 18), to the panels being edge aligned (case 12, Figure 20) and finally to the two panels having a gap of 6 ft between their vertical edges (case 13, Figure 22).

In the case in which the panels are aligned back-to-back (case 10), the flow is practically re-circulated in the region situated in between the panels. In fact, the second panel is situated completely in the wake flow of the first (upstream) panel. As also observed from Figure 16a, the

region between the two panels is characterized by very low pressure levels. The pressure levels in the recirculation region behind the second panel (see also Figure 16c) are relatively low but still higher than the ones in the region between the two panels. This explains why the wind load is negative for the second panel (see also Figure 17c). Observe also the TKE is strongly amplified in the separated shear layers originating at the four edges of the first panel. There is practically no separated shear layer forming at the edges of the second panel as the flow is already separated.

The pressure distribution on the upstream face of the first panel (Figure 17b) is very similar to the one expected when only the first panel is present as the incoming airflow does not "feel" the presence of the second panel. The pressure distribution is very close to uniform on the upstream face of the second panel. The pressure levels are around 18 psf over most of the panel surface. On the other hand the pressure distributions on the back of the two panels are more nonuniform. On the back side of the first panel the pressure increases slightly toward the vertical edges while on the back of the second panel the pressure distribution is similar to the one expected for isolated panels with a circular region of relatively high pressure levels at the center of the panel (~ -6 psf). The very low values of the pressure on the back side of the first panel explain why the mean pressure difference is 34.02 psf, higher than the one observed for any of the isolated panels in the previous cases. As already discussed, the direction of the resulting load on the second panel is toward the incoming flow, however the magnitude of the pressure difference is only 10.36 psf. As the structural design is function only of the magnitude of the pressure induced forces, the second panel is not exposed to high winds. This makes sense, as in effect the first panel "protects" the second one from the impact with the strong air flow. Of course, if the wind direction changes, the roles of the two panels are reversed. So, back-to-back panels have to be designed for a slightly higher wind load compared to isolated ones.

In case 11, the flow becomes non-symmetric. Half of the second panel (12 ft) is protected by the first panel, while the other half is exposed to the incoming airflow. One should mention that besides the wind loads on the two panels, the moments are important for these cases. These moments are high especially on the second panel where the pressure force on the exposed part is positive and of high magnitude, while the force on the part situated behind the first panel is

negative and of relatively low magnitude. These conditions induce a vertical moment of high magnitude.

In the region where the two panels are back to back the pressure distribution (Figure 18a) is similar to the one in case 10. The pressure levels are slightly higher on the back side of panel 1 that is not situated in front of panel 2. This explains why the mean pressure difference on the front panel is slightly smaller in case 11 (31.95 psf) compared to case 10 (34.02 psf). As the two panels are not situated back to back, part of the incoming airflow that is moving directly toward the unexposed part of panel 2 is diverted to the right in the space between the two panels. The velocities in the slot between the two panels are actually very high as the airflow discharge is relatively large while the distance between the two panels is relatively low. This also explains the strong amplification of the TKE in Figure 18b. The other regions of high TKE amplification are in the separated shear layer forming from the edge of panel 1 on the outward side (right relative to the incoming flow direction in Figure 18b) and in the one forming from the edge of panel 2 again on the outward side (left, relative to the incoming flow direction). The two recirculation eddies observed behind the second panel are of unequal sizes and strengths. This is again a consequence of the flow non-symmetry induced by the relative position of the two panels.

The pressure distribution on the front side of the first panel (Figure 19b) is again very similar to the one expected for an isolated panel. The same is true for the half of panel 2 that is directly exposed to the flow. Of course, the other half side of the front of panel 2 is subject to very low pressure induced by the depression created by the fact that panel 1 is in front of part of panel 2. On the back side of panel 1 the pressure are the lowest again in the depression region where the two panels are back to back. Then the pressure increases slightly on the half side of panel 1 that is not in front of panel 2. The pressure distribution is relatively uniform on the back side of panel 2. The distribution of the pressure difference is shown in Figure 19c. In contrast to case 10, the wind load is oriented in the positive streamwise direction. This is because of the pressure wind load on the half side of panel 2 exposed to the incoming airflow. The wind load on the other half of the panel is negative and of relatively low magnitude. Still, despite the small values

of the resultant force on this panel, the rotation moment induced by the forces on the two halves of the panel can be quite high and should be taken into account in the structural design process.

In case 12 the panels are aligned edge by edge but still not situated in the same x=constant plane. Still, the overall pressure distribution starts resembling more to the case where two panels are situated in the same plane and a small slot opening is situated between them (e.g., see case 2). As the two panels are not situated in the same plane, part of the incoming flow is diverted (toward the right relative to the incoming flow direction) as it approaches the second panel in the slot situated in between the vertical edges of the two panels. In this region the flow velocities are very high and separation occurs from the edge of panel 1 (see Figure 20c). As a result the TKE is also strongly amplified in this region (Figure 20b). Interestingly, besides the upstream part of the two separated shear layers originating at the outward edges of the two panels, there is a third region of high TKE amplification situated behind the first panel in the wake flow region. In fact, one can speak of only one wake region that extends in the region behind the two panels rather than two separate ones.

As the incoming flow direction is perpendicular to both panels and there is very little shielding effect, the pressure distributions and pressure levels on the front sides of the two panels are very similar. On the back faces, the main difference is observed on the half side of panel 1 where the pressure levels are lower compared to the case of an isolated panel (Figure 21a). Due to the high velocity values in the slot between the two panels, the pressure values are the lowest in the slot region behind the first panel. This is the reason why the mean pressure difference is higher on panel 1 (34.2 psf) compared to panel 2 (25.5 psf).

In case 13 the gap between the two panels is both laterally (6 ft) and in the streamwise direction (6.67 ft). Except for the additional airflow and non-symmetry induced by the gap between the planes containing the panels in the streamwise direction, the flow is similar to the one studied in case 3. The pressure distributions on the front sides of the two panels are very similar (Figures 22a and 23b) and close to the ones observed in case 3. The main differences occur on the back of the two panels and are mainly due to the direction of the airflow in the space between the two vertical edges of the two panels in the gap region. As also shown by the streamline patterns in

Figure 22c, the jet like flow in between the two panels is oriented at an angle of around 45 degrees with the incoming flow direction. This is the reason the sizes of the two recirculation eddies behind each of the panels are not equal. Again, the relatively large velocities in the jet like flow region, induce the decay of the pressure to levels that are lower to the ones expected to be present in the case of isolated panels. On the panels, the lowest pressure levels are observed on the half side of the back of panel 1 situated toward the jet like flow. The pressure distribution on the back of sign 2 is similar to the one expected for an isolated panel. As a result of the pressure distributions on the front and back sides, the distribution of the pressure difference for panel 2 (Figure 23c) is relatively similar to the one expected for an isolated panel. The mean pressure difference is 29.58 psf which is quite close to the one obtained in case 3 (28.78) for panels of identical dimensions. On the other hand, because of the lower pressures on part of the back side of panel 1, the mean pressure difference is higher for panel 1 (34.2 psf). Also there is a rotation moment associated with the non-symmetrical pressure distribution on panel 1.

4.d Investigation of the effect of the presence of add-on exit signs

The presence of small add-on exit signs was investigated for the case in which the main panel sign had a height of 8.5 ft and a width of 22.5 ft. In the case 14 simulation only the main sign was present while in the case 15 simulation both the main sign and the add-on sign situated on the top left of the main sign were present. The pressure distributions on the two faces of the panels and the distributions of the pressure differences in cases 14 and 15 are shown in Figures 24 and 25, respectively. The presence of the add-on sign does not alter significantly the pressure distribution on the main panel. In fact the mean pressure difference on the main panel is very close in the two cases (32.06 vs. 31.27 psf). The mean pressure difference on the add on sign is only slightly smaller (30.32 psf).

4.e Investigation of the effect due to the passage of trucks

One of the concerns of the Iowa DOT was whether or not the forces acting on the signs, (in particular on thick signs), change considerably when trucks are passing underneath. In this case the trucks in fact act as additional obstructions in the way of the regular airflow which is

accelerated in the openings between the top of the trucks and the sign. This is the main reason the simulation corresponding to case 16 (1 main rectangular panel 10.17 ft high, 32 ft wide and 6.42 ft wide with two trucks passing beneath) was undertaken. The relative position and dimensions of the panel and the trucks are shown in Figure 26. Figure 26 also shows the pressure distribution on the back side of the panel and the trucks (for simplicity the thickness of the trucks was taken equal to the one of the panel). These distributions are qualitatively similar to the ones observed for isolated signs of similar aspect ratio.

Figure 28 shows the pressure contours, streamwise velocity contours, 2D streamline patterns and TKE contours in a vertical plane cutting through the middle of one of the trucks. The same quantities are shown in a horizontal plane cutting through the middles of the panel sign in Figure 29. As a result of the presence of the truck between the ground level and the bottom of the panel sign, two air-flow jet like regions are present between the truck and the panel and between the truck and the ground level (Figure 26). For the same reason, the recirculation region behind the panel sign is non-symmetrical (Figure 28c). The TKE is strongly amplified in the separated shear layer forming from the top horizontal edge of the sign. The amplification of the TKE is smaller in the separated shear layer forming from the bottom edge of the panel sign, because of its interaction with the airflow jet and with the weaker separated shear layer originating on the top horizontal edge of the truck. The pressure distribution in the same plane (Figure 27) looks qualitatively similar to the one observed for isolated signs. In the horizontal plane, the flow remains symmetric with respect to the symmetry plane of the sign. This is because the two trucks are positioned in a symmetrical way with respect to the midlle of the sign.

It appears that for the particular geometry considered, the presence of the trucks underneath the sign results in a slight reduction of the mean pressure difference (~24.6 psf) on the sign compared to the value expected for the case the sign is isolated. This does not necessarily mean that for all situations the passage of the trucks would not induce additional loads on the panel. Probably considering a case in which the correct length of the trucks and their relative position to the sign is taken into account is worse pursuing. The flow patterns may be much more complicated than in the case studied here.

4.f Investigation of the effect of air holes in a rectangular panel

The effect of the air holes was investigated through comparison of the results of two computations of the air flow past a rectangular panel of aspect ratio 1:2. In the first simulation the panel did not have any holes, while in the second one the panel has two arrays of three holes. The holes were disposed in a collocated manner (see Figure 2). The other dimensions in Figure 2 are L1=0.7H, L2=0.3H, L3=0.35H, L4=0.3H and W=2.0H. Using the non-dimensional length scale H, the surface of the panel was $2H^2$. The diameter of each hole was 0.1H. The total surface of the six holes was $0.045H^2$. The holes area represents only 2.5% of the total panel surface. Both simulations were run at a Reynolds number of $Re=UH/\nu=150{,}000$ such that the differences in the pressure distributions and the total wind load are due solely to the presence of the holes.

The mesh is visualized in characteristic sections in Figures 30 and 31. The typical size of the computational cell in the holes area is 0.005H (~30 wall units). Around the panel the size of the cells is around 0.015H (~100 wall units). The panel thickness is 0.02H. The size of the computational domain around the panel (vertically and laterally) is about 30D. The total length of the computational domain is around 80D.

A considerable amount of time was spent making sure one can generate a high quality mesh for this problem and the boundary layers on the panel are resolved with sufficient resolution. The final mesh in the two simulations contains close to 1.5 million hexahedral cells. The unstructured mesh (panel with holes) was generated using a paving technique which allows rapid variation in the characteristic size of the elements (e.g., observe the reduction in the element size around the holes for the panel with holes) while maintaining a high overall quality of the mesh and low stretching ratios.

The flow patterns obtained in the two simulations are compared in Figures 32 to 35 in a vertical plane cutting the two panels through the middle (the plane intersects the middle holes on the top and bottom rows) and in Figures 36 to 39 in a horizontal plane cutting through the middle of the two panels (the plane does not intersect the two rows of holes). Figures 32 and 36 show

streamlines. Figures 33 and 37 show the pressure contours (same contour scale is used in both computations). Figures 34 and 38 show the contours of the streamwise velocity (the streamwise direction corresponds to the incoming wind direction). Finally, Figures 35 and 39 show the distribution of the turbulent kinetic energy (TKE) that characterizes the local intensity of the velocity fluctuations due to turbulence.

As expected, the flow fields, including the recirculation regions behind the panels, remain symmetrical with respect to the vertical and horizontal symmetry axis of the panels (see Figures 32 and 36). In both simulations two large symmetrical vortices are forming on both sides of the symmetry plane. However, the presence of the holes, and the associated formation of small jets, induces the formation of two small vortices downstream of these holes for the simulation of the airflow past the panel containing holes. The pressure contours in Figures 33 and 37 show, as expected, that the largest pressure values are observed on the upstream face of the panel. This is because the presence of the panel induces the formation of adverse pressure gradients. As a result of these adverse pressure gradients, the flow velocity decays toward zero as the panel is approached. Behind the panel, where the flow is recirculating with a relatively small velocity compared to the free-stream (wind) velocity, the pressure values are much lower and the pressure gradients milder. Again this is expected to happen in the wake past a bluff body.

The presence of the holes increases the mean pressure levels in the recirculating flow present behind the panel with holes compared to the pressure levels observed behind the panel without holes. Observe that the largest levels in the wake behind the panel with holes are observed just behind the holes, which is expected as the flow velocity through the holes is very high (couple of times higher than the free stream velocity). This results into an overall smaller force on the panel in the case of the panel with holes compared to the case of the panel without holes. The non-dimensional mean pressure difference between the two faces of the panel is 0.856 (~35 psf – the relative high value of the mean pressure difference for the panel without holes is due mainly to the fact that the Reynolds number is considerable lower compared to the other simulations) for the panel without holes and 0.664 (~ 27.18 psf) for the panel with holes. The difference is about 20%. This is very significant as the total area of the holes is less than 2.5% of the panel surface. Adding more holes or enlarging their section should result in an even larger reduction of the total

mean pressure force on the panel. The challenge is in disposing the holes in such a way that the writing is still visible and the light through the holes does not reduce the readability of the writing on the panel sign. We have several ideas how to address these problems.

The turbulence kinetic energy (TKE) in the wake is significantly different in the two simulations. Interestingly, the presence of the holes reduces the TKE levels in the vertical middle plane (Figure 35). This is positive, as the TKE is related to the amplitude of the large scale force oscillations on the panel. In the middle horizontal plane (Figure 39), the TKE is amplified in the wake of the panel with holes. However, this amplification is not very important compared to the simulation of the panel without holes.

5. Conclusions and Recommendations for Future Work

The main goal of the present numerical investigation was to study the pressure distributions and wind loads on typical highway sign and traffic signal structures. A fundamental requirement is to be able to study the interactions among the panel structures for signs with multiple panels accurately estimate the pressure forces on these structures. Steady state fully three-dimensional Computational Fluid Dynamics (CFD) simulations were conducted using a state-of-the-art Reynolds Averaged Navier-Stokes turbulence model of the airflow around these panels to determine the pressure distributions on the two sides of each panel and the distribution of the pressure differences.

The conditions in the simulations were representative of severe wind conditions (wind speed 90 mph) and the wind direction was always perpendicular to the panels. In the present study only the CFD analysis was carried out. However, the present data can be used to conduct a detailed structural analysis of the traffic sign structures. The role of CFD is critical, as it allows obtaining the pressure difference distribution on the whole panel. For panels of complex shapes or for multiple signs panels the pressure distributions can be highly non-symmetrical. As a result, besides the mean force acting on the panel, strong rotational moments can also be present. These moments are practically impossible to estimate using empirical formulae. Accurate estimation of

wind forces and moments on large highway sign structures is important due to possible structural failure of these sign structures under strong winds.

Part of the present study, a parametric study was conducted that allowed to investigate the effects of aspect ratio and sign spacing for regular rectangular panels, the effect of sign depth for the dynamic message signs that are now being used on Iowa highways, the effect induced by the presence of back-to-back signs, the effect of the presence of add-on exit signs, and the effect of the presence of trucks underneath the signs and the ground level. The reduction in the mean pressure force on the panels as a result of the presence of small air holes in a wide rectangular panel was also investigated for one particular design (air holes were disposed in a collocated manner on two rows).

When looking at the mean pressure the results from the numerical simulation are within 20% for practically all the panels without holes studied in the present study. The largest differences were observed for the case of back-to-back signs. The increased mean pressure can perhaps easily be taken into consideration by simply increasing the wind loads obtained by the wind formula by a factor of 20 to 30%. However, since the actual pressure distribution is unsymmetric, large moments are produced as well. It is quite possible that recent premature cracking observed in the dynamic message sign (DMS) panels may in fact be due to additional stresses that are caused by these moments. Moreover, it is very possible that the maximum wind loads (forces and rotational moments) will occur for wind directions which are not necessarily perpendicular to the wind panels. So, for the case of back-to-back and DMS panels, we strongly recommend pursuing a detailed parametric study in which the wind direction is varied.

The presence of small holes (the total area of the holes around 2.5% of the total panel surface) resulted in a considerable reduction (20%) of the wind load force. This is very significant. Thus, we recommend this idea be pursued together with ways to insure that the presence of the holes does not reduce the visibility of the signs. Several ways to address these problems are possible.

The present approach can be also used to estimate wind loads (forces and moments) on large esthetic shape signs that are of interest to Iowa DOT. It is expected the wind loads on these signs

estimated using CFD may be sensibly different than the ones estimated using the empirical formulae used by Iowa DOT for rectangular panels.

We also recommend performing aeroelastic computational modeling of the effects of the wind on the highway sign and traffic signal structures. We propose using advanced finite-element codes (e.g., Ansys) for structural analysis of the typical structures (e.g., cantilevered mast arm traffic signal and its supports) subject to the loads estimated using CFD.

Another important aspect that was not addressed in this preliminary study is the presence of unsteady loads due to the large scale vortex shedding behind the panels. A resonance condition, causing large amplitude relatively steady vibrations of the structure, can occur if the frequency of shedding coincides with a natural vibration frequency of the structure. Vortex-shedding can occur at relatively low wind speeds and thus, even if the structure has enough strength, such large oscillations contribute to premature fatigue failure. Estimation of these dynamic loads requires performing unsteady RANS simulations. Though more computationally expensive, we think this is an important area of future work which will allow a dynamic analysis of the aeroelastic effects.

Related to that, one should point out that the standard code-based design of these structures considers static wind loads based on the expected maximum wind speeds. The AASHTO *Standard Specifications for Structural Supports for Highway Signs, Luminaires and Traffic Signals* (2001 and 2003 interim specifications) have been revised in its entirety through a major research project conducted under the auspices of the National Cooperative Highway Research Program (NCHRP 17-10). The 2003 document includes updated provisions and criteria for extreme wind loads and new provisions and criteria on fatigue design. However, the methods used to obtain the new provisions and criteria in the AASHTO Standard are still essentially based on a static strength design approach. The structures designed in this manner may have adequate factor of safety against strength failure but their response to aeroelastic phenomena is largely unknown. For example, flutter may cause torsional vibrations that usually receive little consideration in design. Buffeting may cause large structural motions and over time can induce fatigue damage. Of course, it is necessary to account for these phenomena as early in the

design/construction cycle as possible. A basic prerequisite is to have a rational understanding of these effects and to develop appropriate procedures and tools that can be used efficiently in the design process. We think an integrated CFD-computational structural design analysis approach can accomplish that. Through this analysis one should be able to evaluate the errors that are made when a simplified steady-state approach is used to estimate the wind loads on these structures.

6. References

ANSYS User's manual, Volumes I, II, and III, Version 10, Swanson Analysis Systems, Inc., Houston, PA, 2005.

ANSYS theory manual, Version 10, Swanson Analysis Systems, Inc., Houston, PA, 2005.

Bhatti, M.A. Advanced Topics in Finite Element Analysis of Structures: with Mathematica and MATLAB Computations, John Wiley, New York 2006.

Bhatti, M.A. Fundamental Finite Element Analysis and Applications: with Mathematica and MATLAB Computations, John Wiley, New York. 2005.

Constantinescu, G.S., Krajewski, W.J., Ozdemir, C.E., and Tokyay, T. (2005). "Simulation of Airflow around Rain Gauges: Comparison of LES with RANS Models," Submitted for Publication to Advances in Water Resources.

Fluent 6.1 User's Guide, Fluent Inc., Lebanon, 2001.

Tokyay, T. and Constantinescu, S.G. (2005b), "Large Eddy Simulation and Reynolds Averaged Navier Stokes Simulations of flow in a realistic pump intake: A validation study," World Water and Environmental Resources Congress, Alaska, May 2005.

APPENDIX

Figure 1: Damage to two highway structures due to high winds

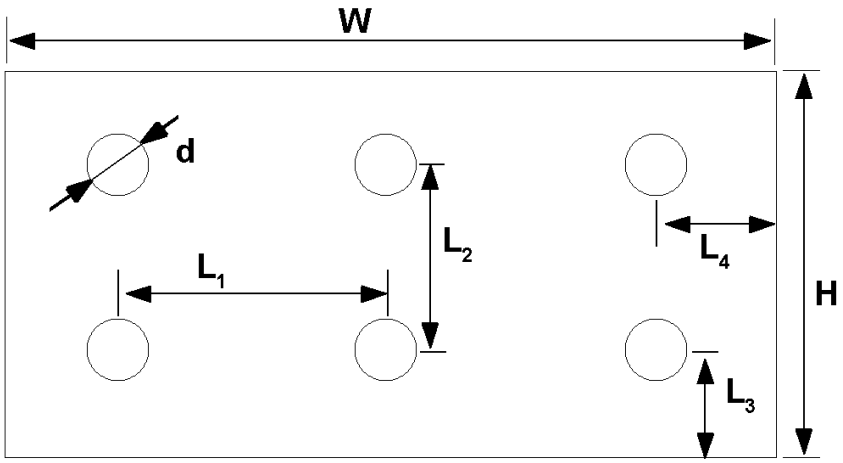

Figure 2. Sketch showing possible disposition patterns for the holes on the panel and main geometrical parameters.

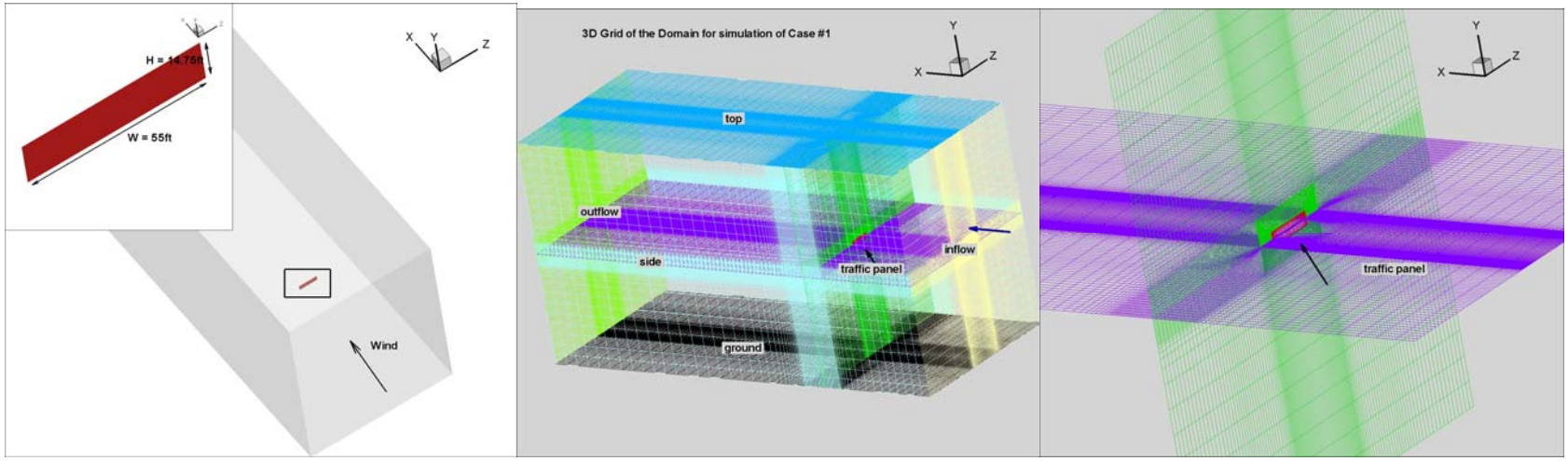

Figure 3. General views of the computational domain and mesh for case 1.

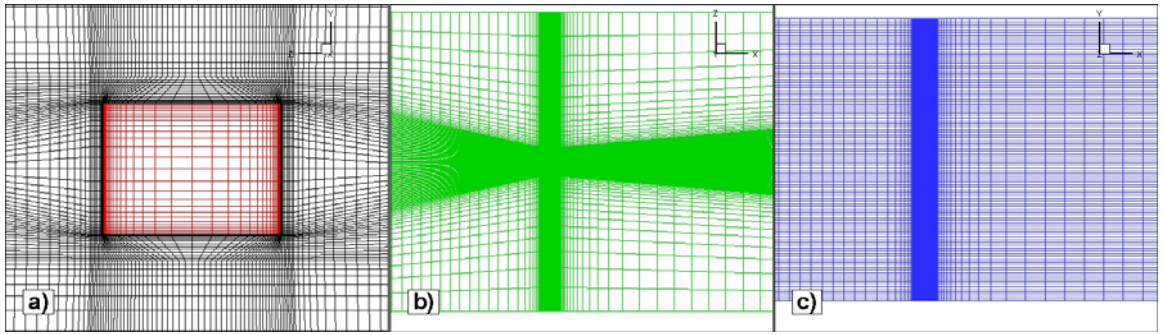

Figure 4. General view of the mesh; a) in a plane perpendicular to the flow, b) in a plane parallel to the bottom of the domain, c) in a plane parallel to the sides of the domain.

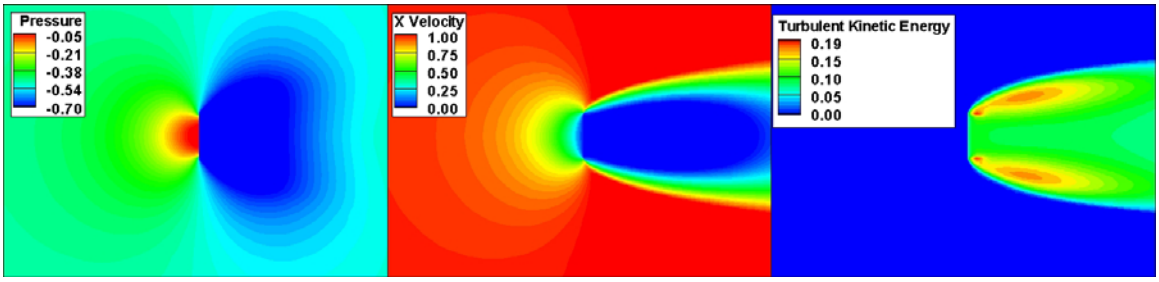

Figure 5. Pressure (left), streamwise velocity (middle) and TKE (right) distributions in a vertical plane cutting through the symmetry axis of the panel in case 1.

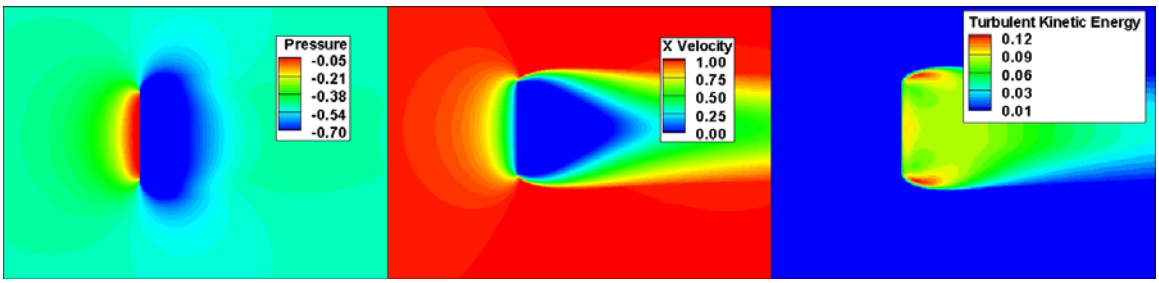

Figure 6. Pressure (left), streamwise velocity (middle) and TKE (right) distributions in a horizontal plane cutting through the symmetry axis of the panel in case 1.

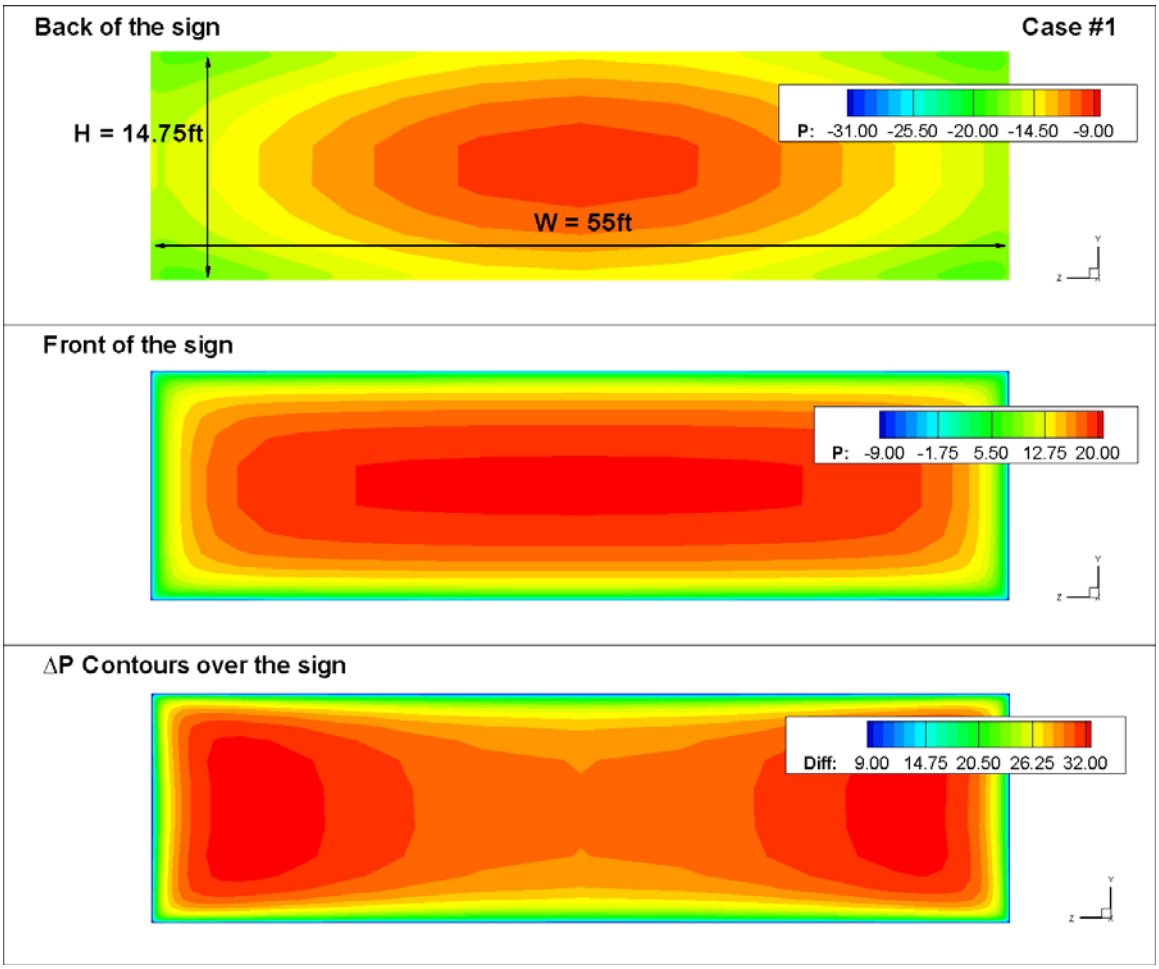

Figure 7. Distributions on the back side pressure (top), the front side pressure (middle) and the pressure difference between the two sides (bottom) for case 1. The dimensional pressure levels (psf) are shown.

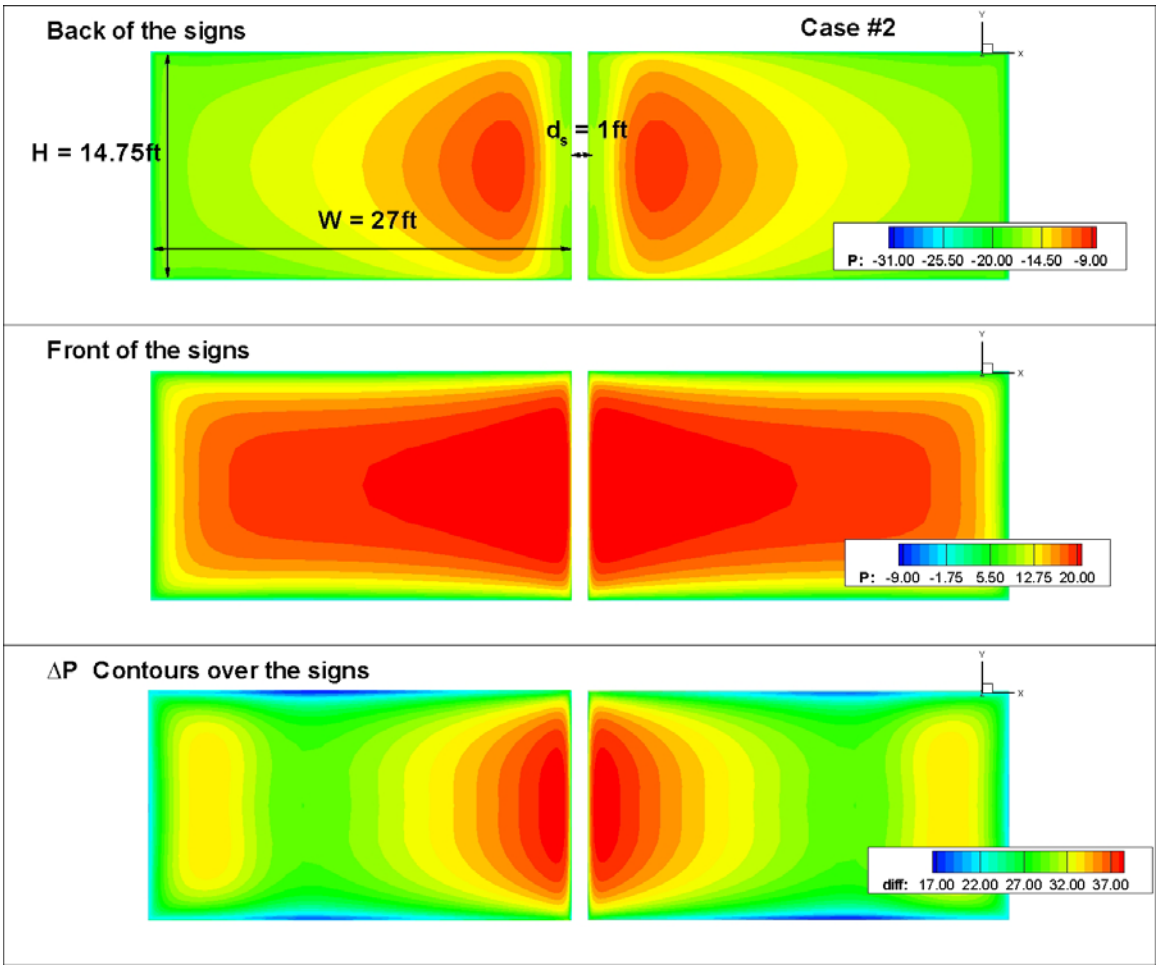

Figure 8. Distributions on the back side pressure (top), the front side pressure (middle) and the pressure difference between the two sides (bottom) for the panels considered in case 2. The dimensional pressure levels (psf) are shown.

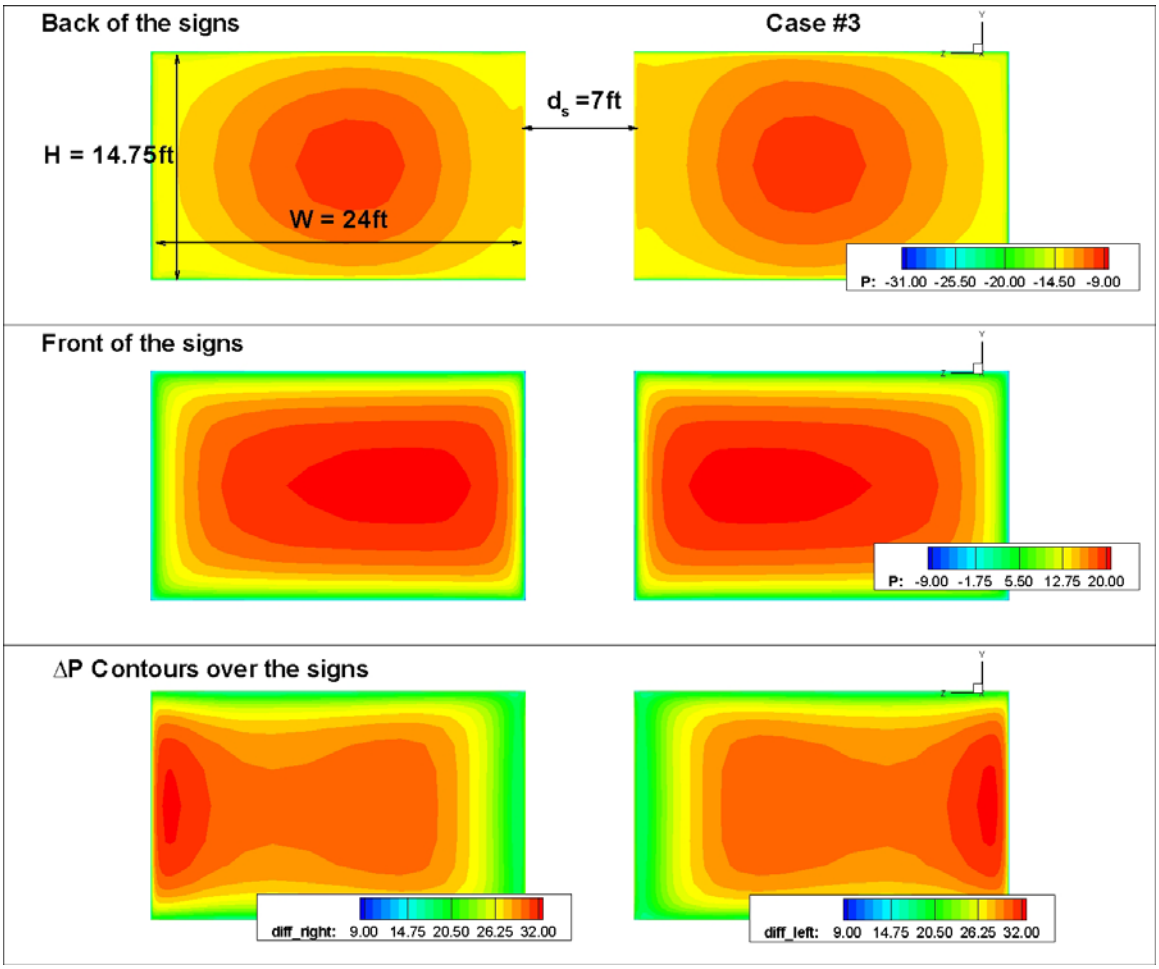

Figure 9. Distributions on the back side pressure (top), the front side pressure (middle) and the pressure difference between the two sides (bottom) for the panels considered in case 3. The dimensional pressure levels (psf) are shown.

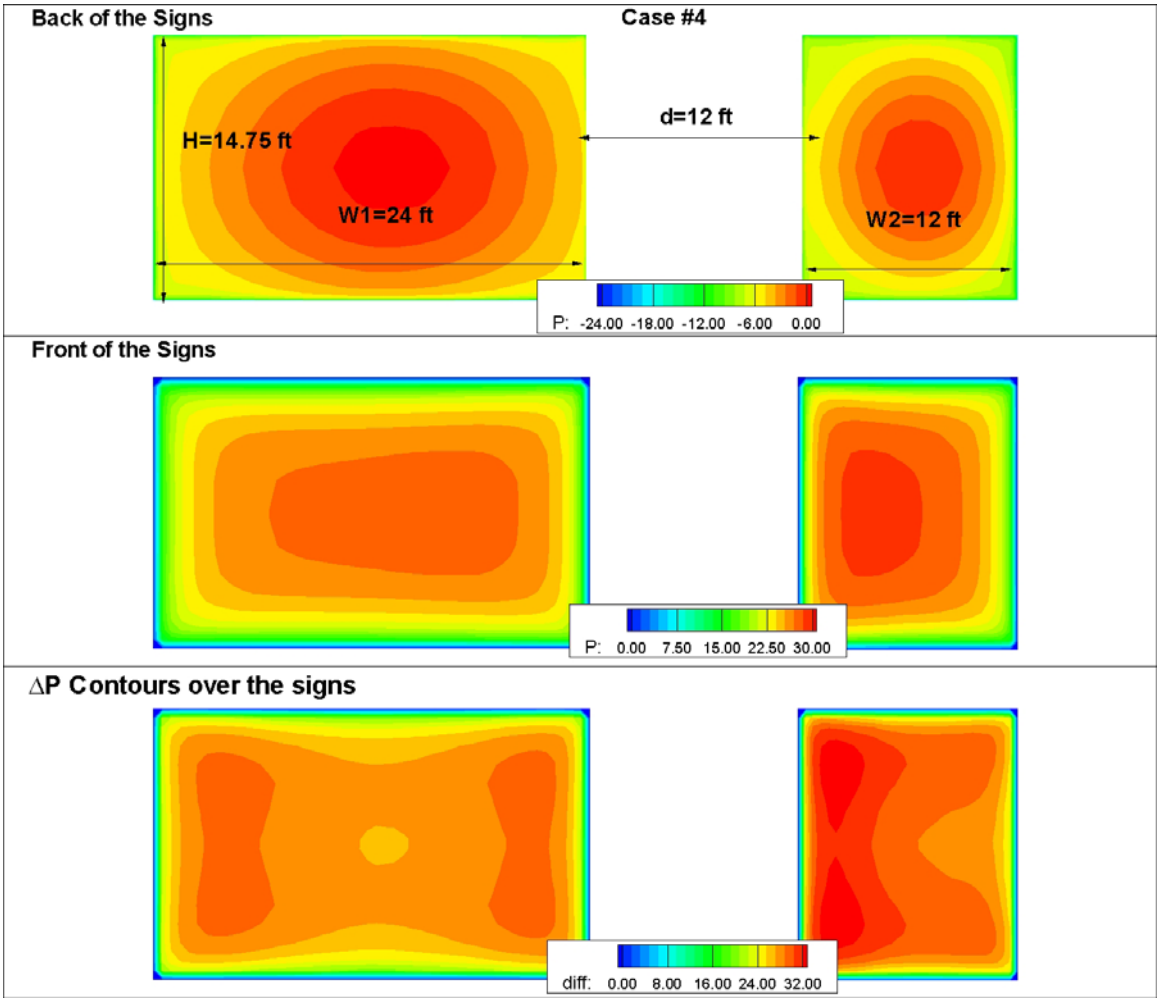

Figure 10. Distributions on the back side pressure (top), the front side pressure (middle) and the pressure difference between the two sides (bottom) for the panels considered in case 4. The dimensional pressure levels (psf) are shown.

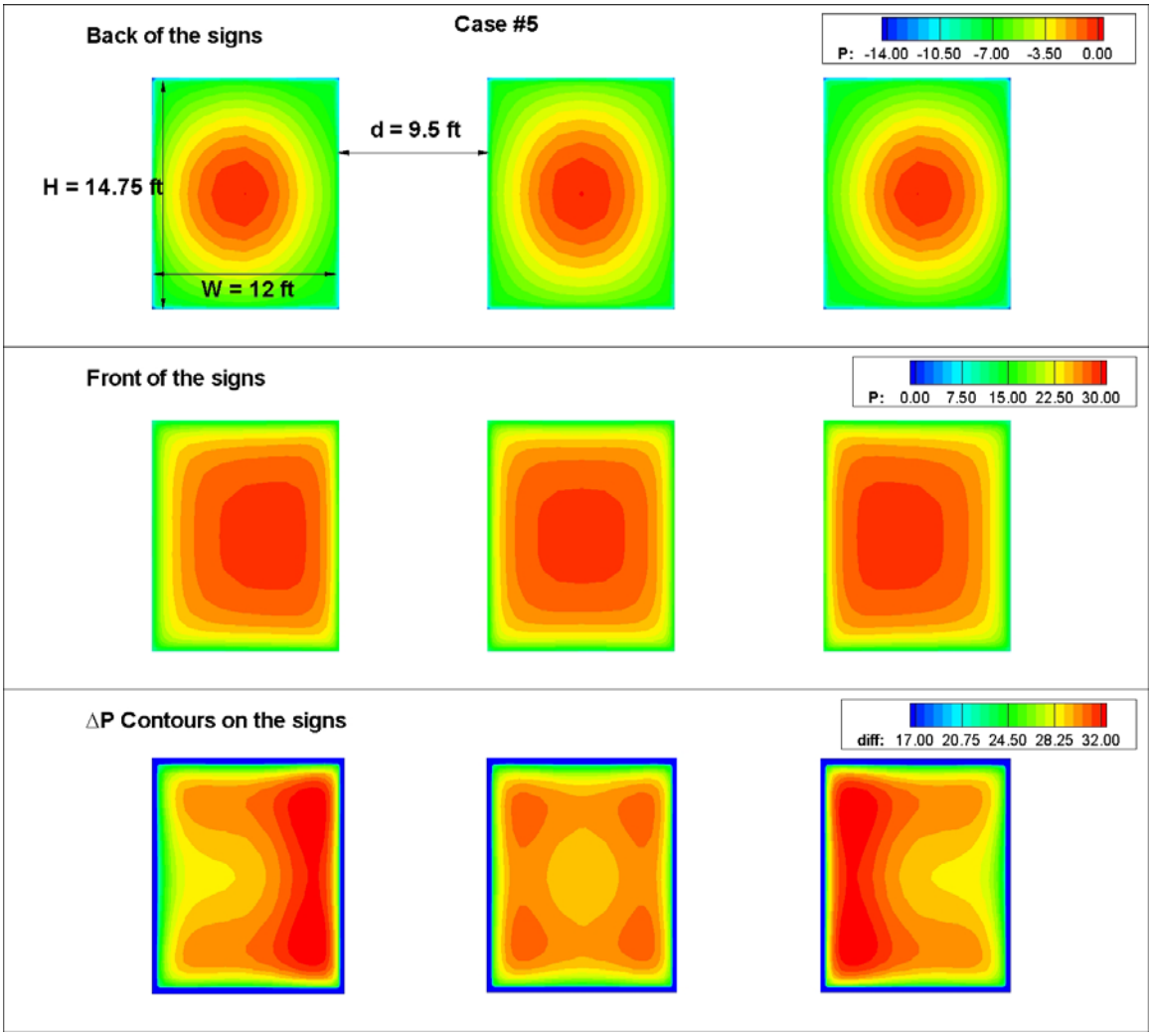

Figure 11. Distributions on the back side pressure (top), the front side pressure (middle) and the pressure difference between the two sides (bottom) for the panels considered in case 5. The dimensional pressure levels (psf) are shown.

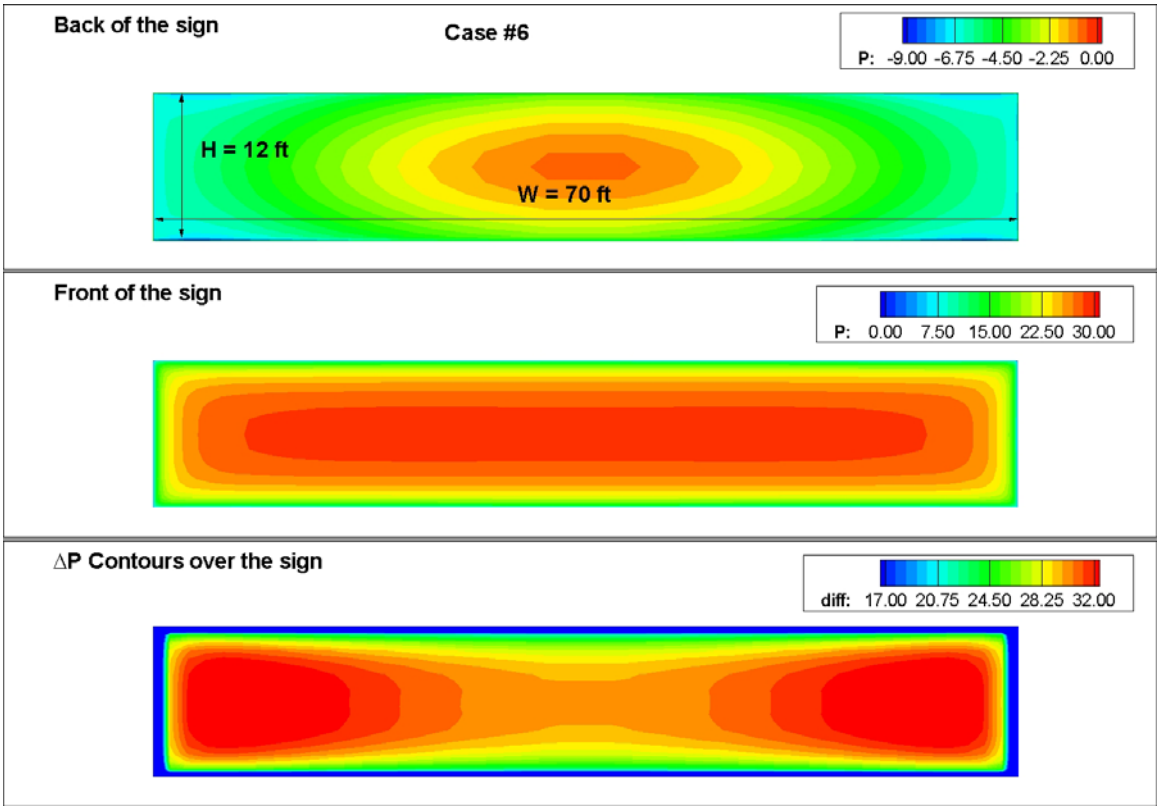

Figure 12. Distributions on the back side pressure (top), the front side pressure (middle) and the pressure difference between the two sides (bottom) for the panels considered in case 6. The dimensional pressure levels (psf) are shown.

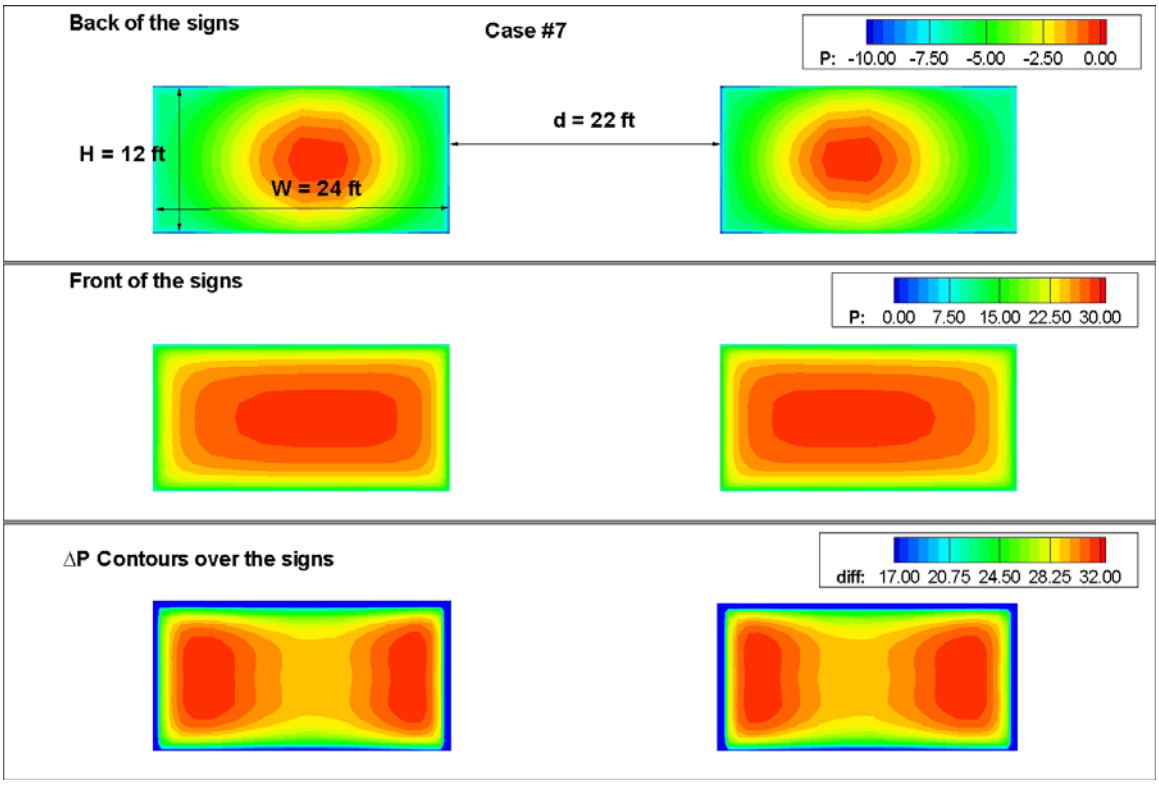

Figure 13. Distributions on the back side pressure (top), the front side pressure (middle) and the pressure difference between the two sides (bottom) for the panels considered in case 7. The dimensional pressure levels (psf) are shown.

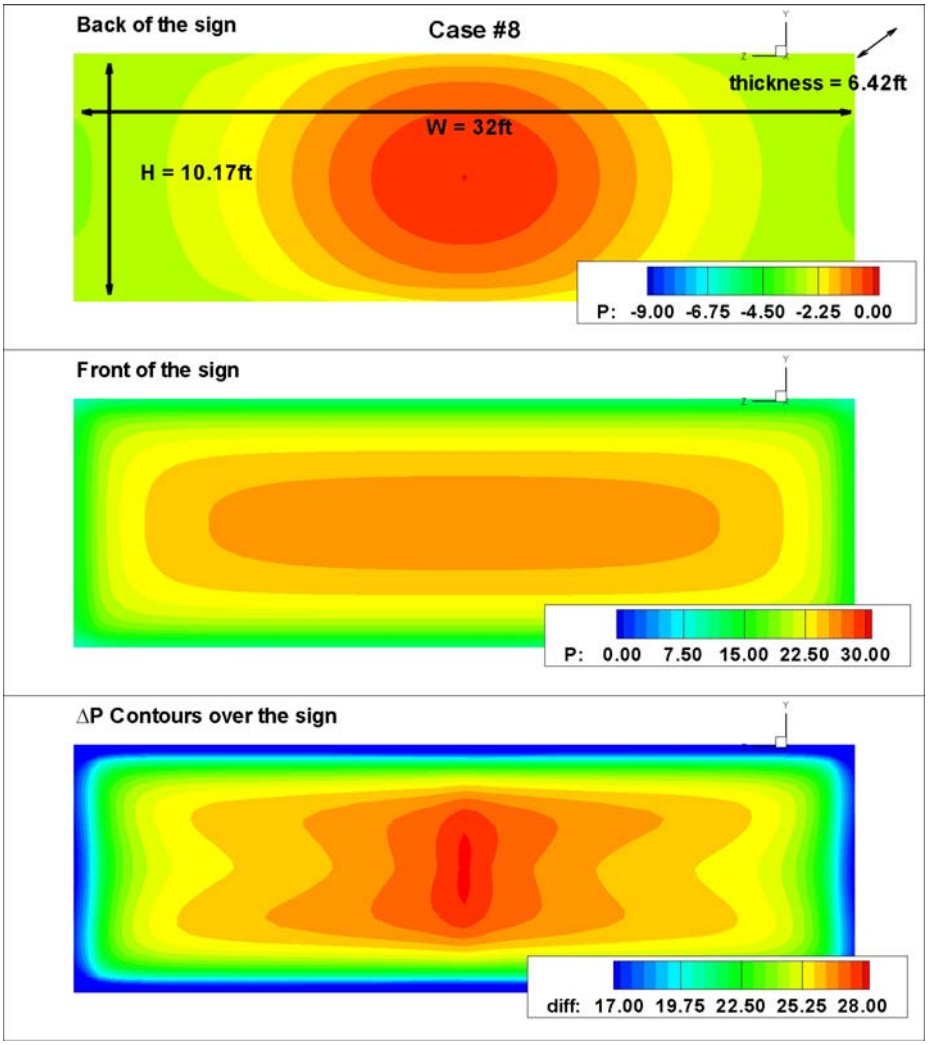

Figure 14. Distributions on the back side pressure (top), the front side pressure (middle) and the pressure difference between the two sides (bottom) for the dynamic message sign considered in case 8. The dimensional pressure levels (psf) are shown.

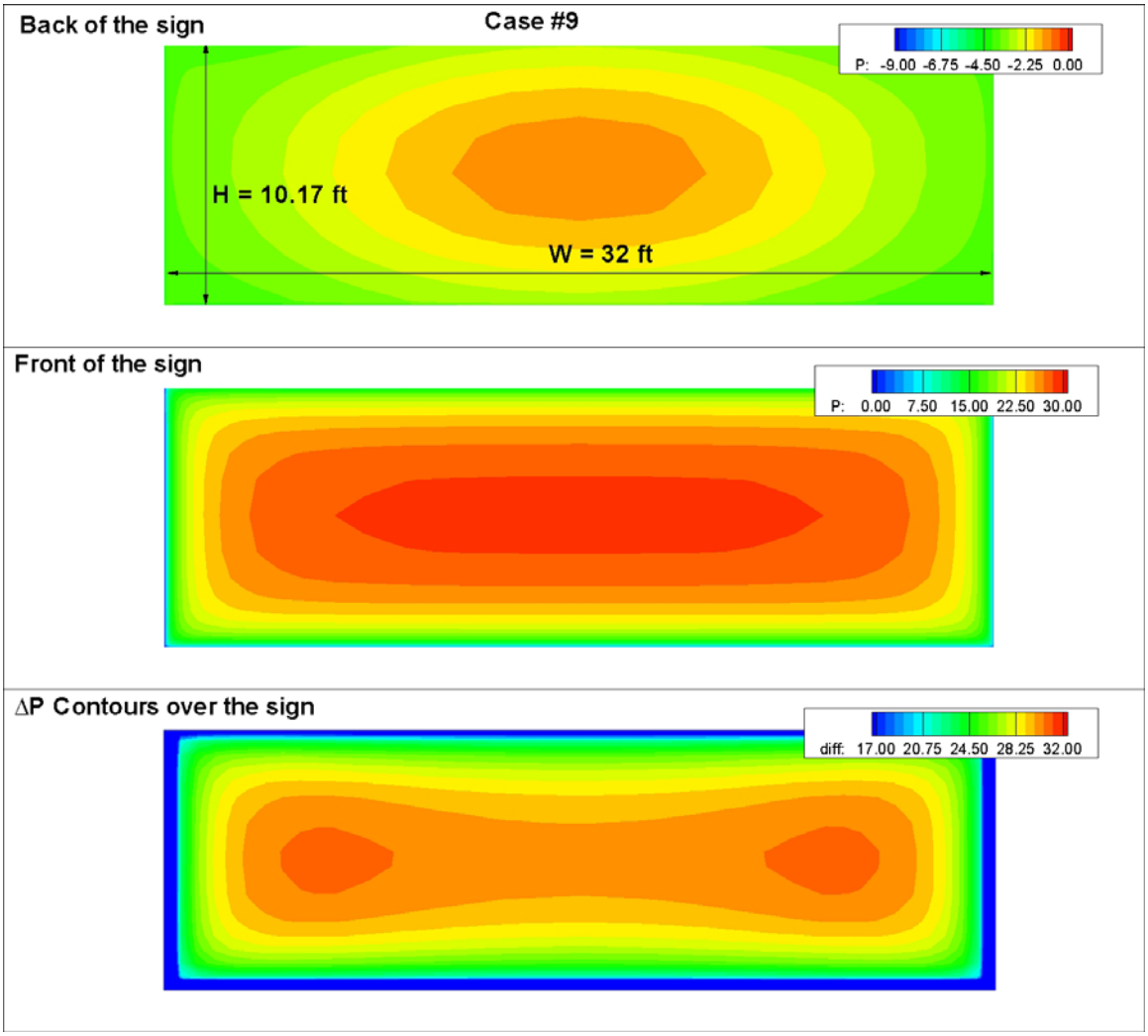

Figure 15. Distributions on the back side pressure (top), the front side pressure (middle) and the pressure difference between the two sides (bottom) for the thin panel considered in case 9. The dimensional pressure levels (psf) are shown.

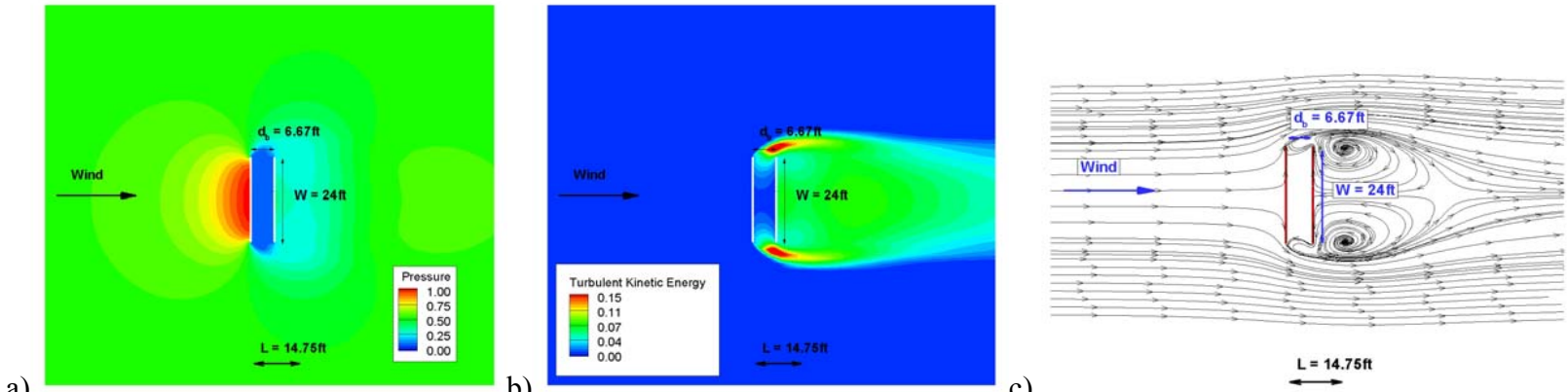

Figure 16. Visualization of the solution for case 10 in a horizontal plane cutting at mid-height level through the center of the panels; a) non-dimensional pressure contours, b) TKE contours, c) streamlines.

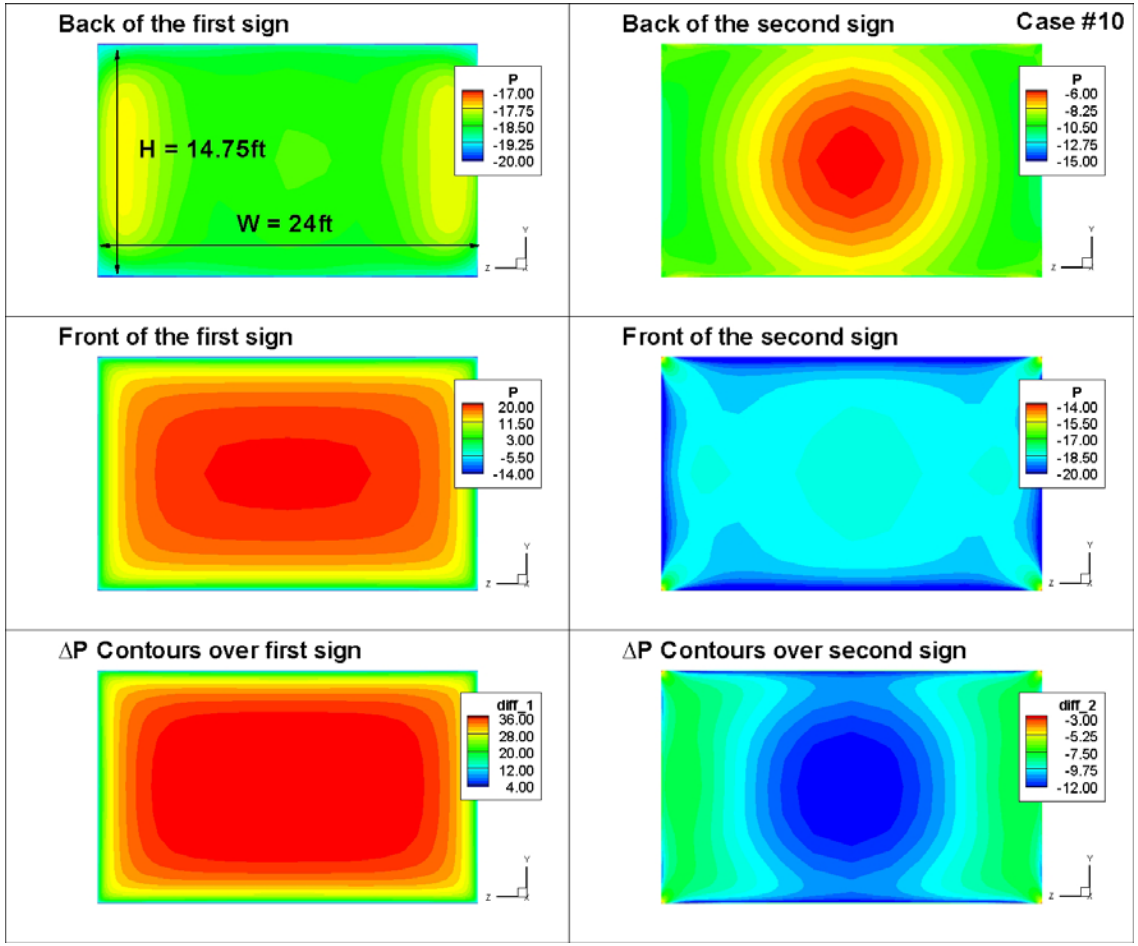

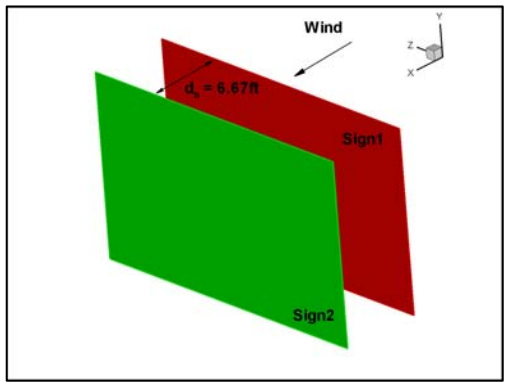

Figure 17. Distributions on the back side pressure (top), the front side pressure (middle) and the pressure difference between the two sides (bottom) for the panels considered in case 10. The dimensional pressure levels (psf) are shown. The relative position of the two panels is shown in the sketch.

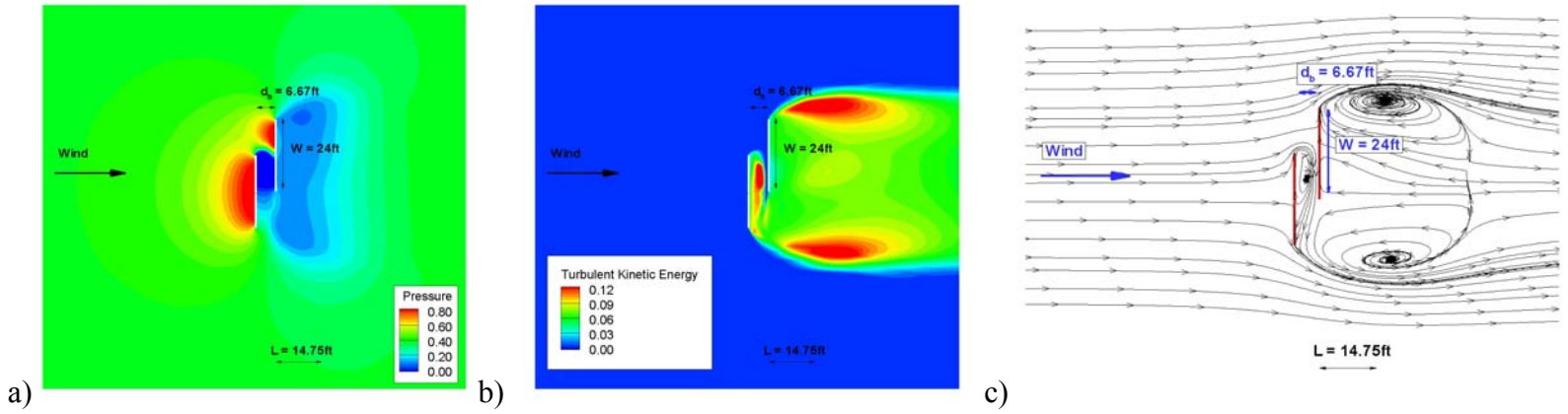

Figure 18. Visualization of the solution for case 11 in a horizontal plane cutting at mid-height level through the center of the panels; a) non-dimensional pressure contours, b) TKE contours, c) streamlines.

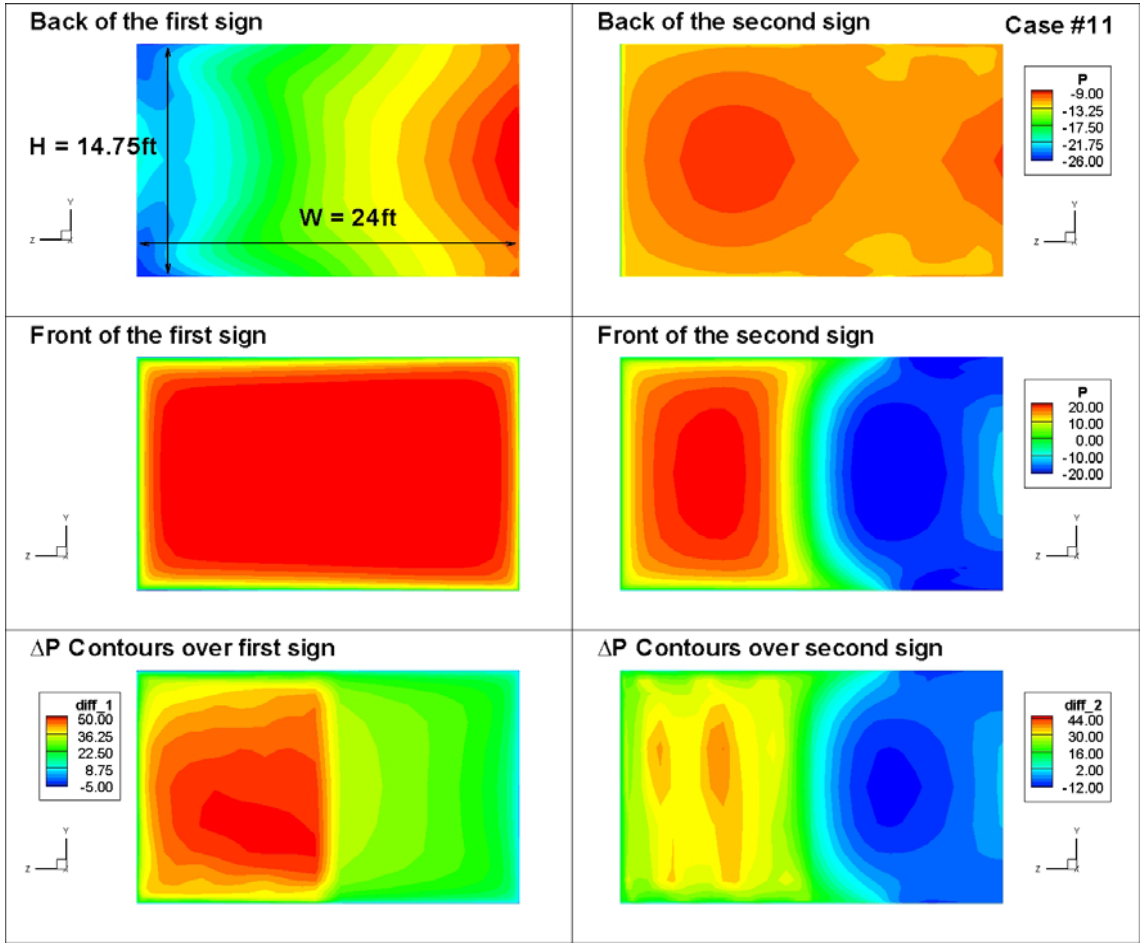

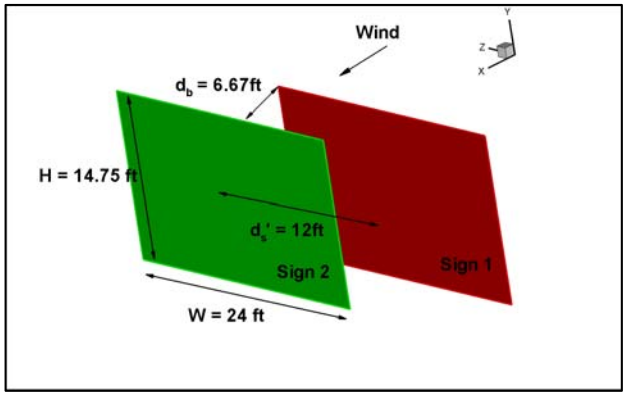

Figure 19. Distributions on the back side pressure (top), the front side pressure (middle) and the pressure difference between the two sides (bottom) for the panels considered in case 11. The dimensional pressure levels (psf) are shown. The relative position of the two panels is shown in the sketch.

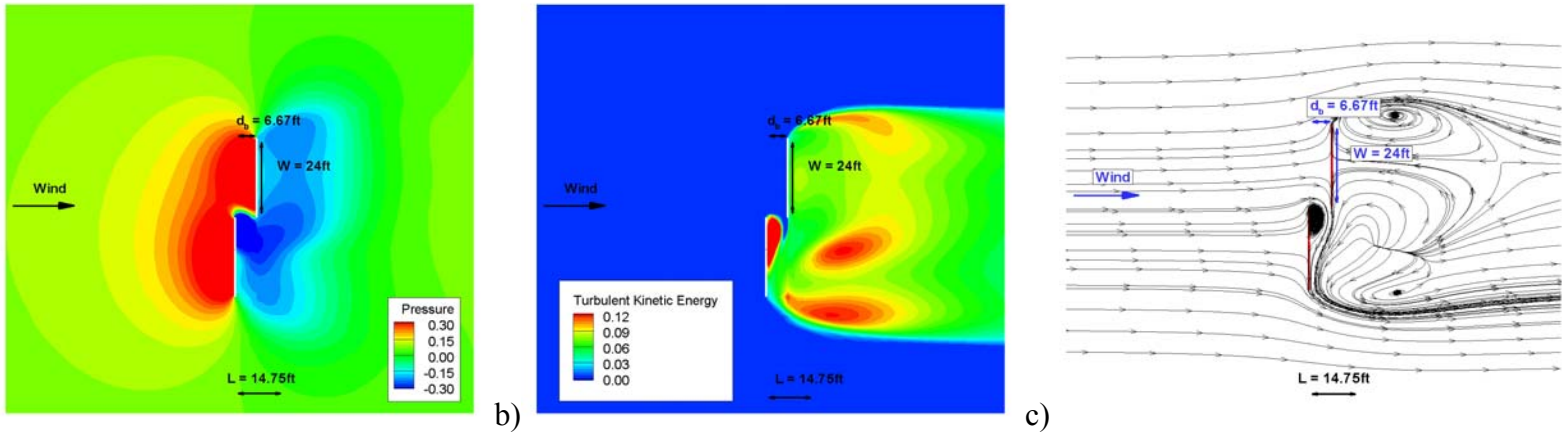

Figure 20. Visualization of the solution for case 12 in a horizontal plane cutting at mid-height level through the center of the panels; a) non-dimensional pressure contours, b) TKE contours, c) streamlines.

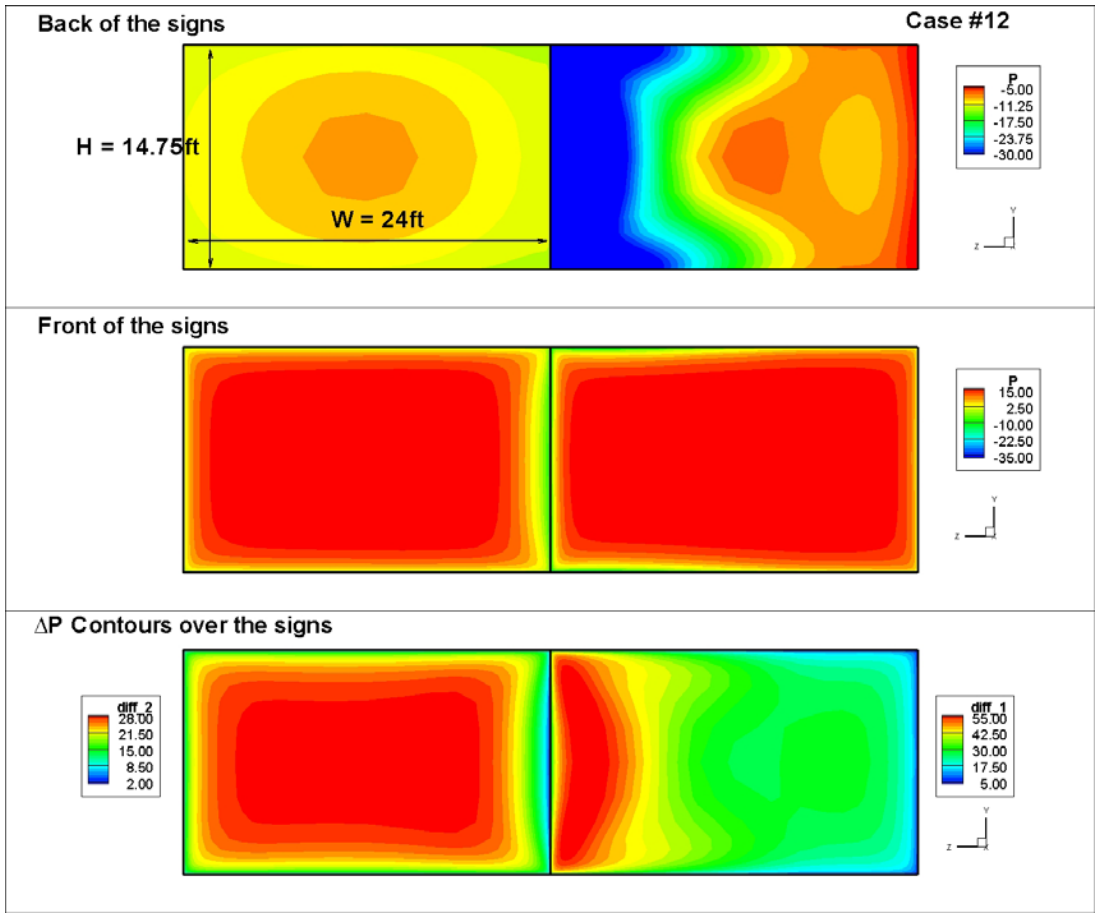

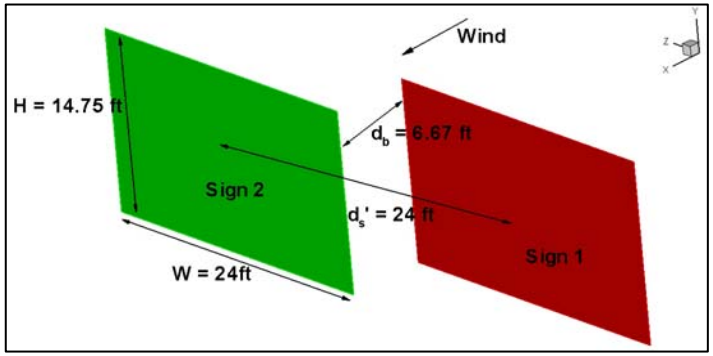

Figure 21. Distributions on the back side pressure (top), the front side pressure (middle) and the pressure difference between the two sides (bottom) for the panels considered in case 12. The dimensional pressure levels (psf) are shown. The relative position of the two panels is shown in the sketch.

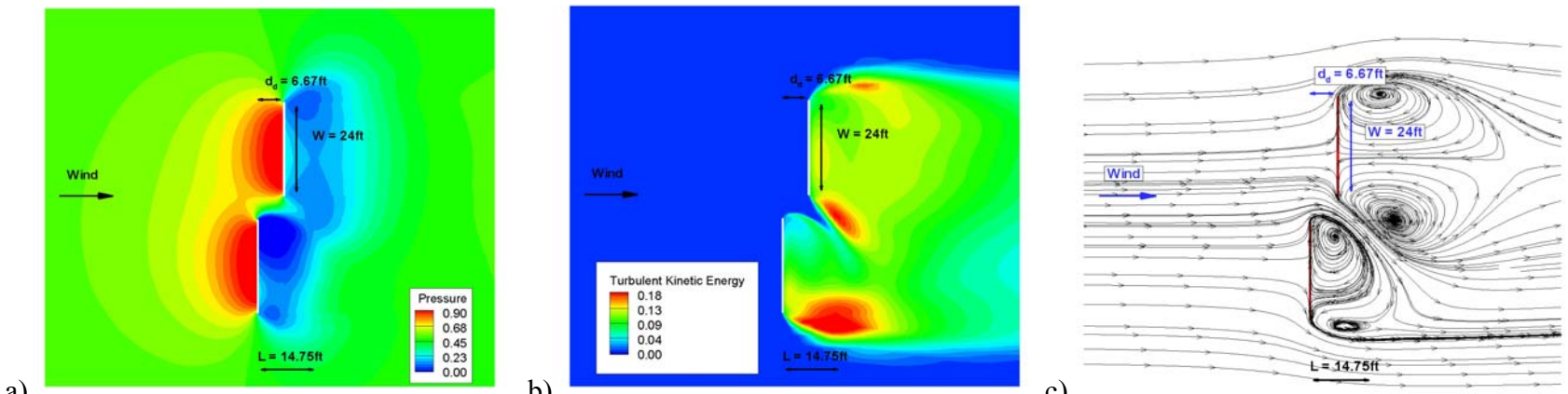

Figure 22. Visualization of the solution for case 13 in a horizontal plane cutting at mid-height level through the center of the panels; a) non-dimensional pressure contours, b) TKE contours, c) streamlines.

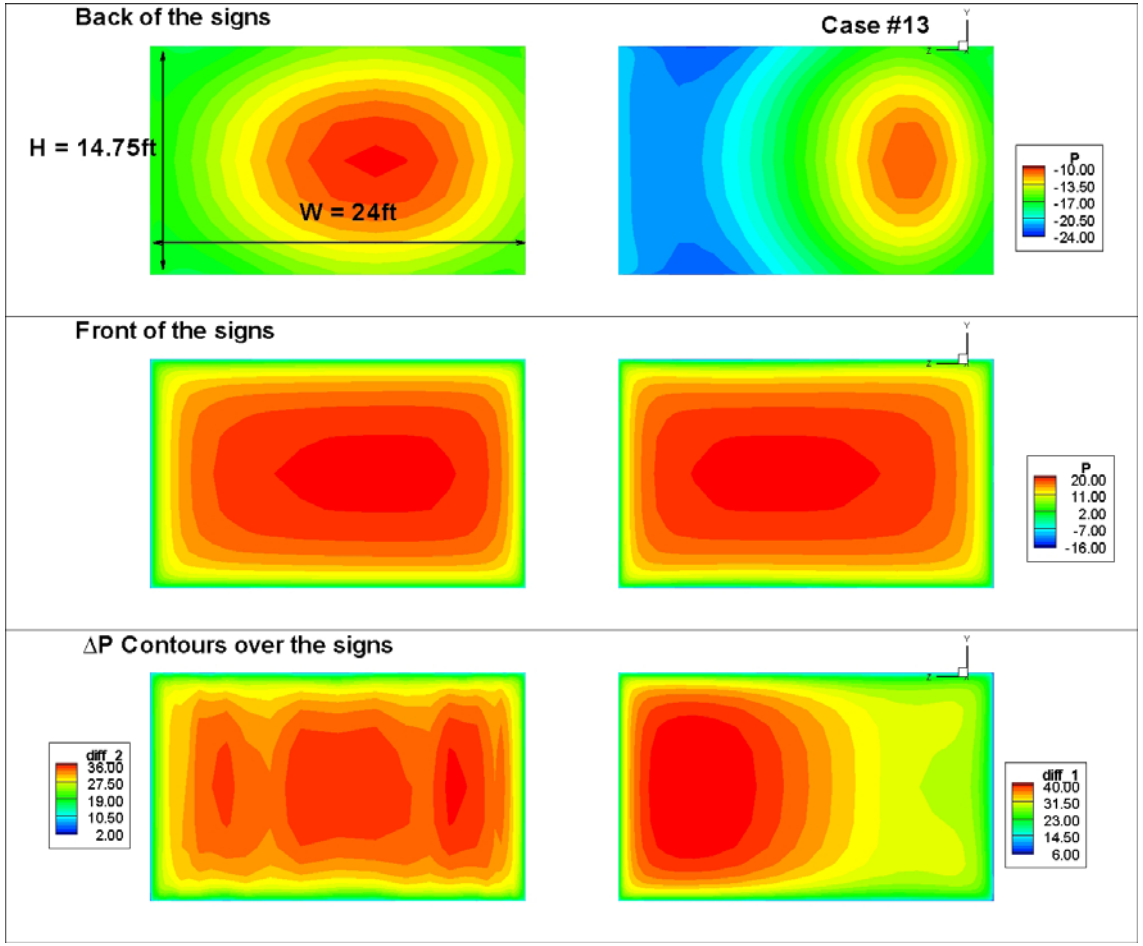

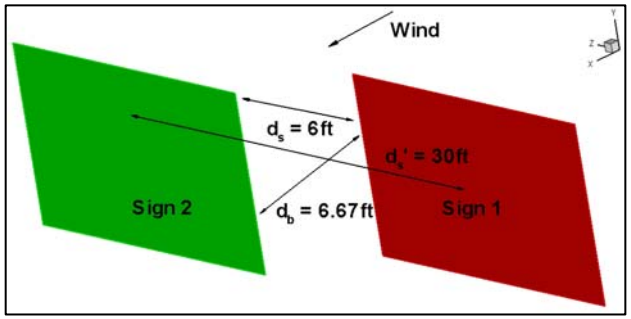

Figure 23. Distributions on the back side pressure (top), the front side pressure (middle) and the pressure difference between the two sides (bottom) for the panels considered in case 13. The dimensional pressure levels (psf) are shown. The relative position of the two panels is shown in the sketch.

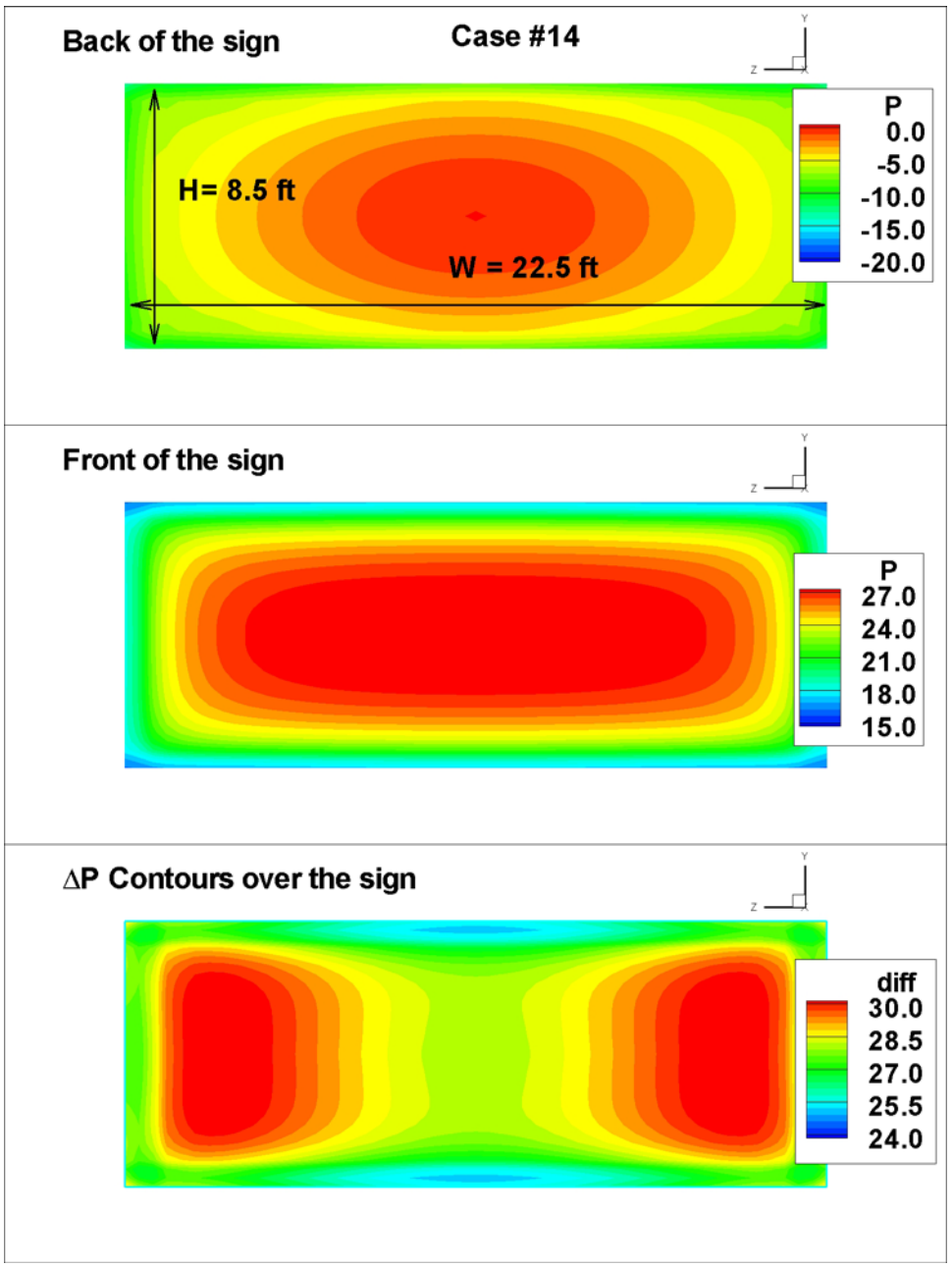

Figure 24. Distributions on the back side pressure (top), the front side pressure (middle) and the pressure difference between the two sides (bottom) for the panel considered in case 14. The dimensional pressure levels (psf) are shown.

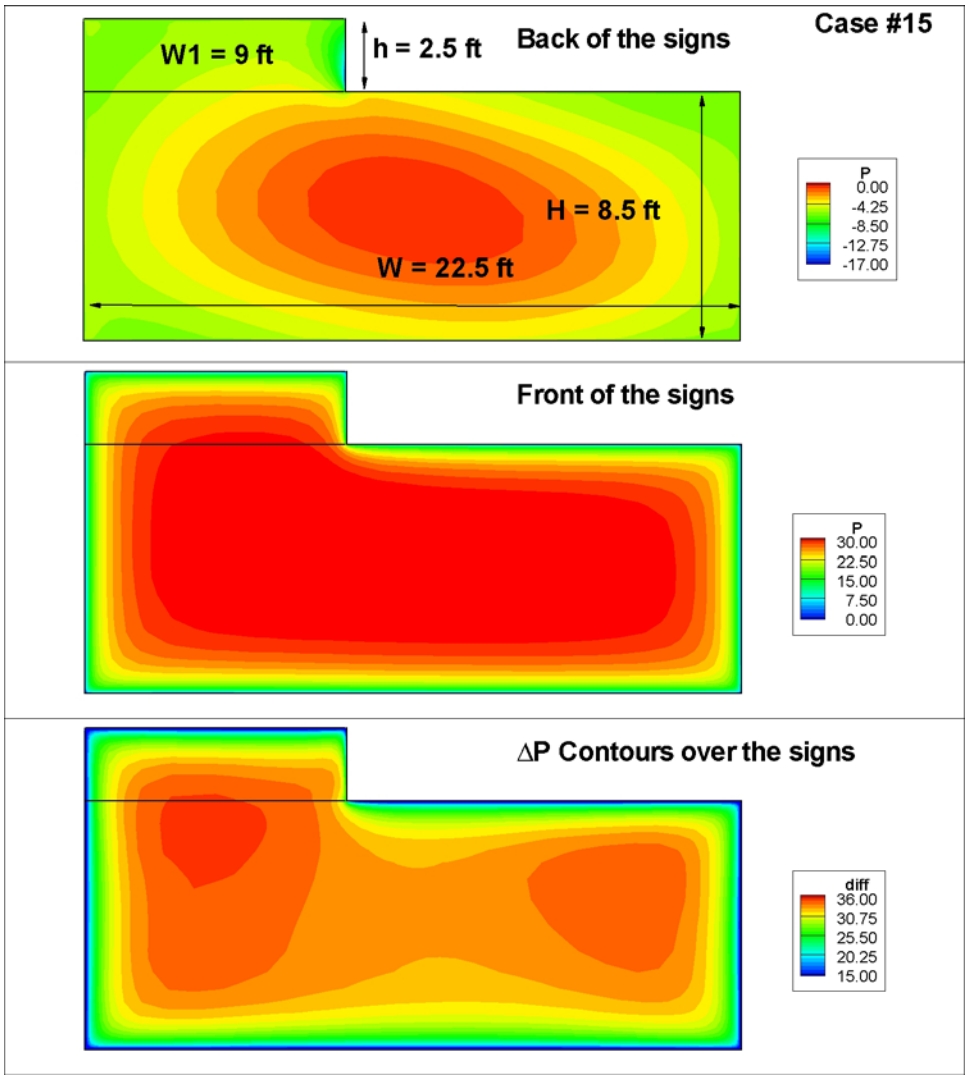

Figure 25. Distributions on the back side pressure (top), the front side pressure (middle) and the pressure difference between the two sides (bottom) for the panel with an add-on sign considered in case 15. The dimensional pressure levels (psf) are shown.

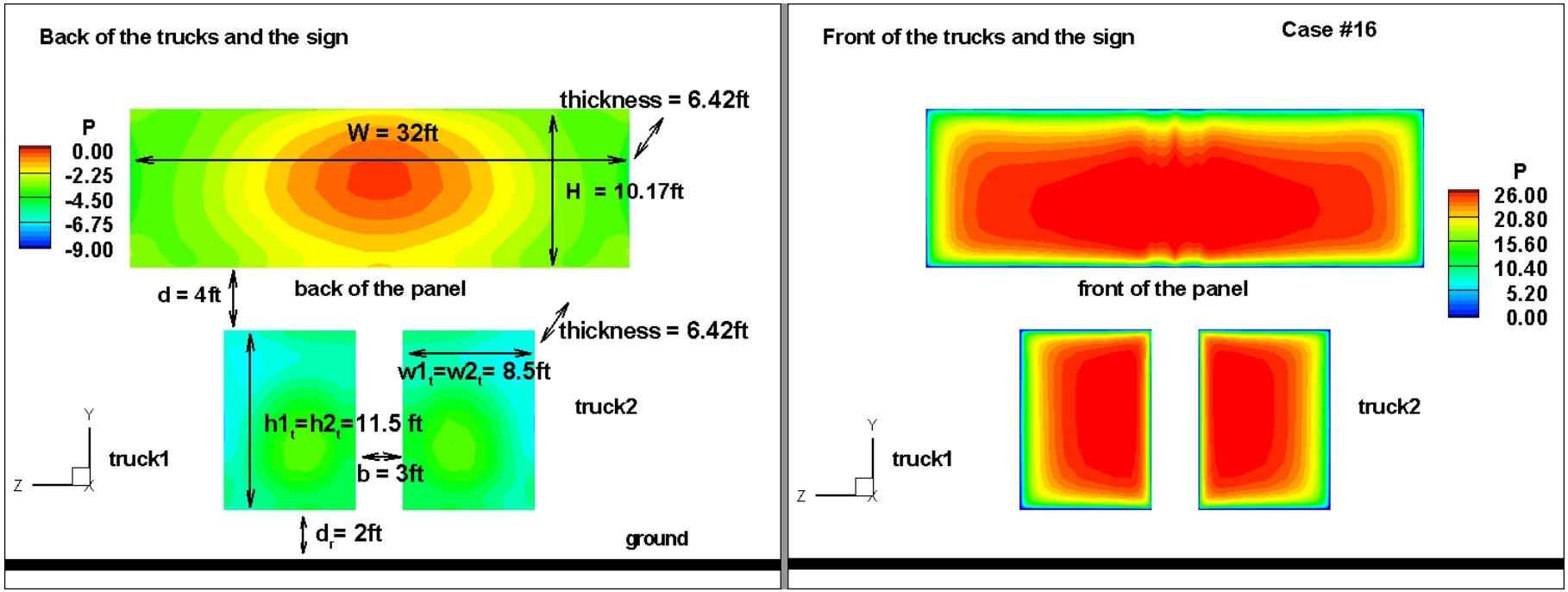

Figure 26. The relative position of the panel and the two trucks in case 16.

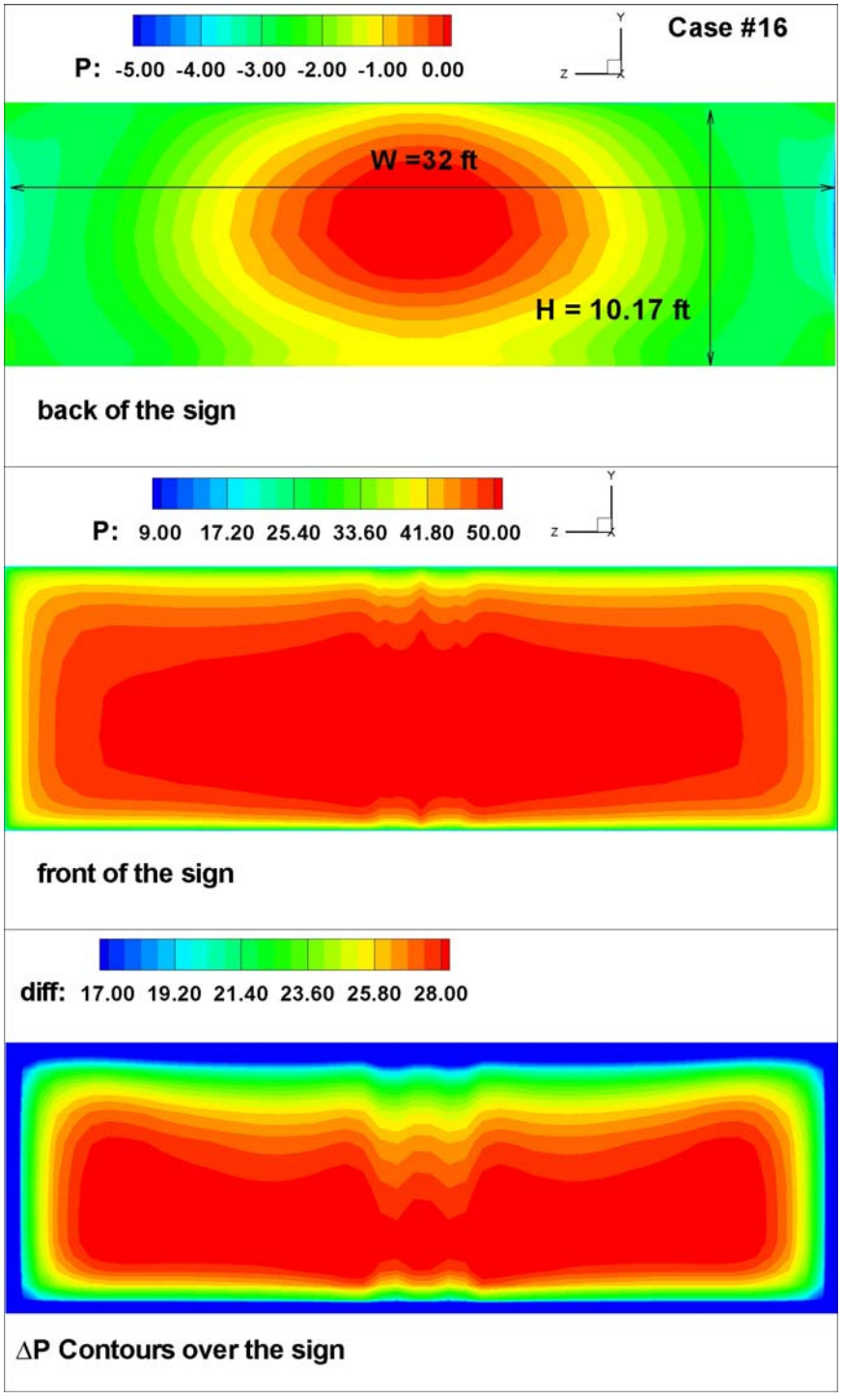

Figure 27. Distributions on the back side pressure (left) and the front side pressure (right) for the panel and the two trucks considered in case 16. The dimensional pressure levels (psf) are shown. The relative position of the panel and the two trucks is indicated in the figure.

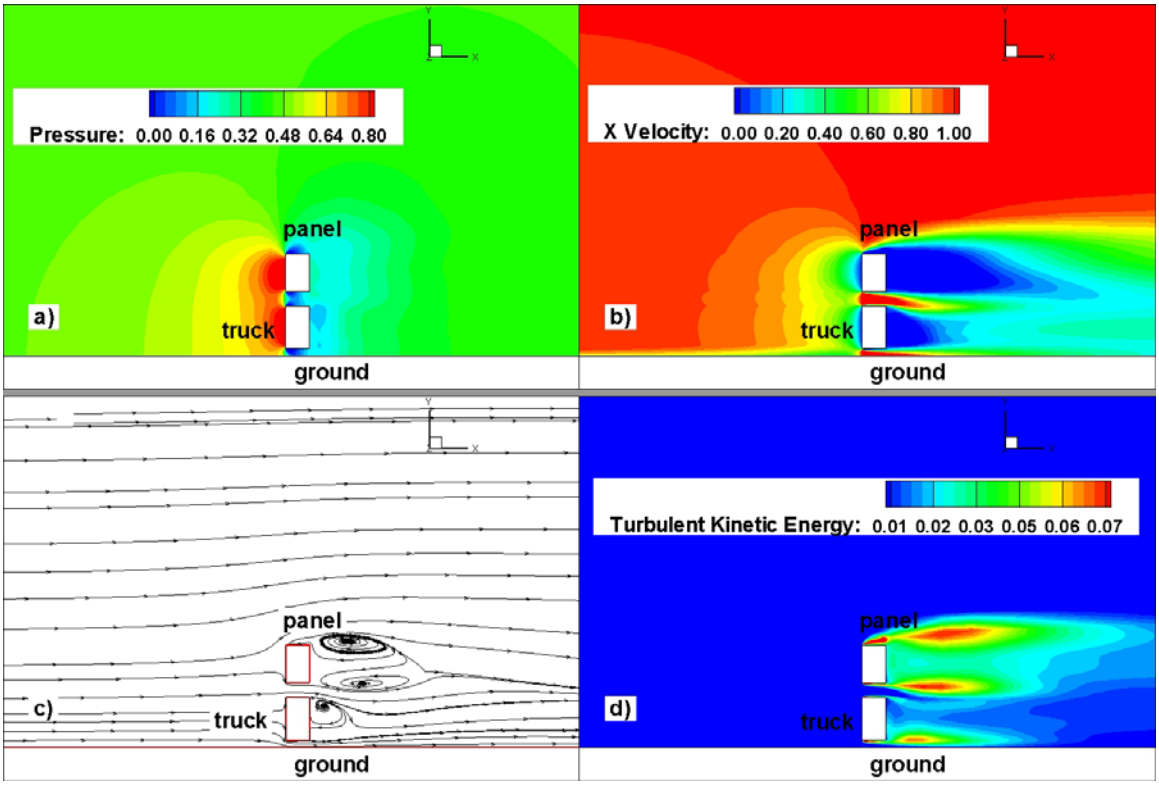

Figure 28. Visualization of the numerical solution for case 16 in a vertical plane cutting through the middle of one of the trucks. a) pressure contours; b) streamwise velocity contours; c) 2D streamline patterns; d) TKE contours.

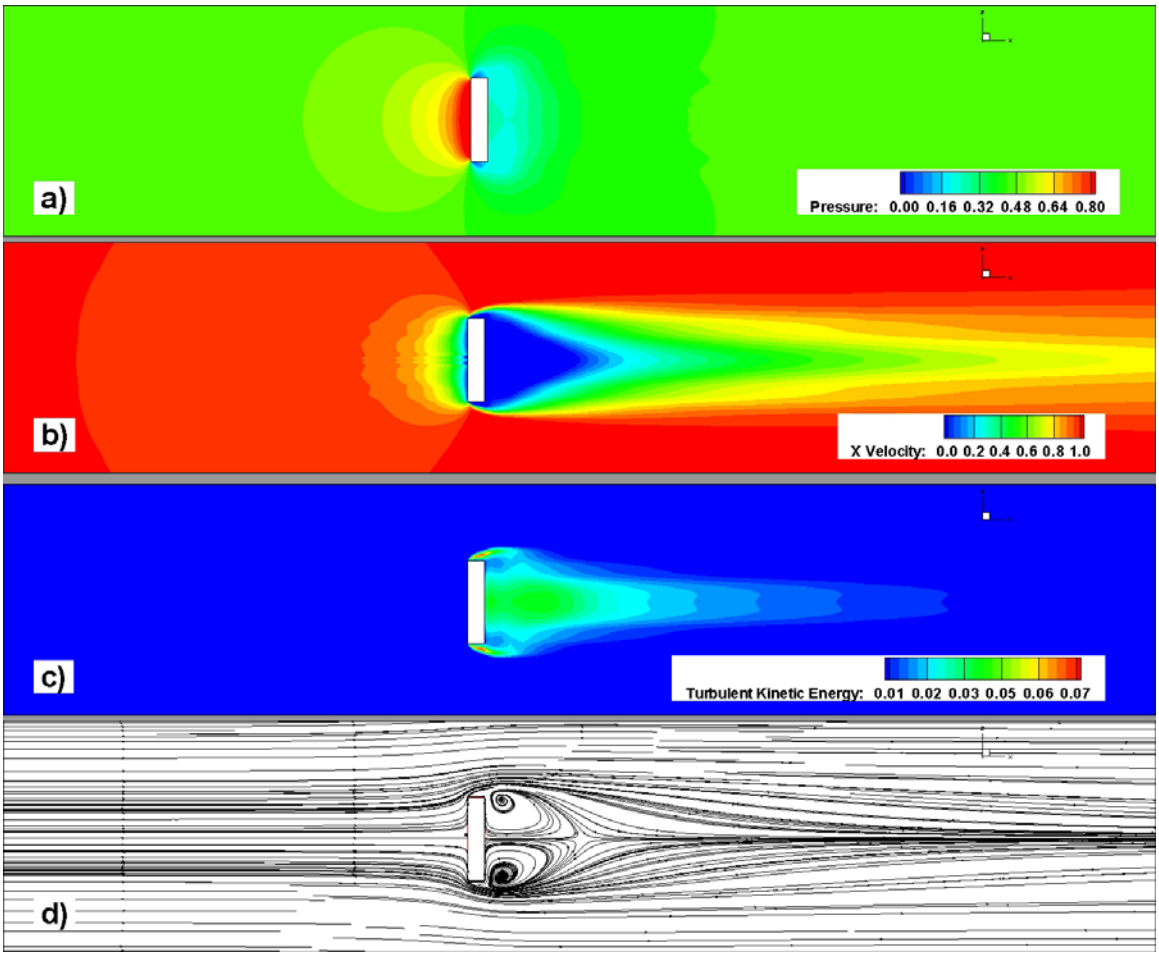

Figure 29. Visualization of the numerical solution for case 16 in a horizontal plane cutting through the middle of the panel sign. a) pressure contours; b) streamwise velocity contours; c) 2D streamline patterns; d) TKE contours.

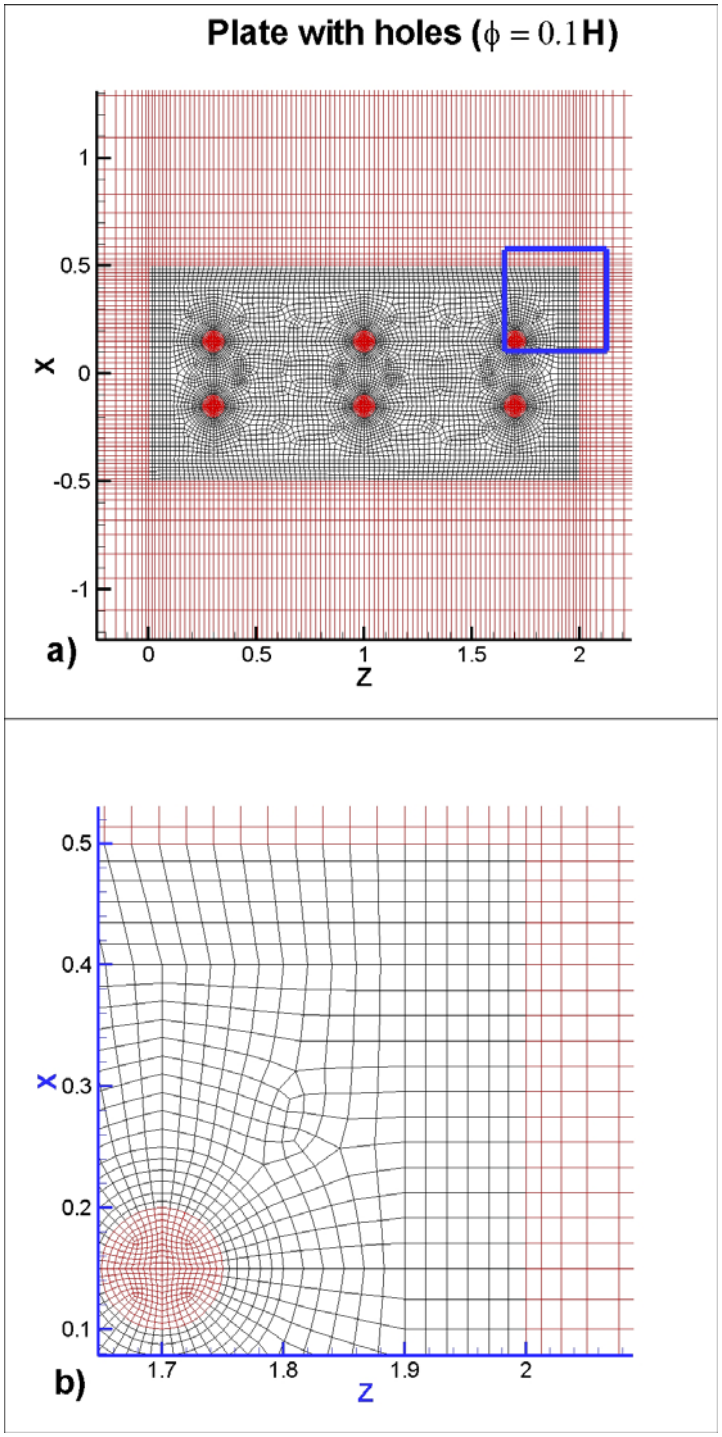

Figure 30. Visualization of the computational mesh for panel with holes in a spanwise plane. a) the mesh on the panel and around it, b) detail near one of the holes showing the transition from the hole region to the surrounding domain.

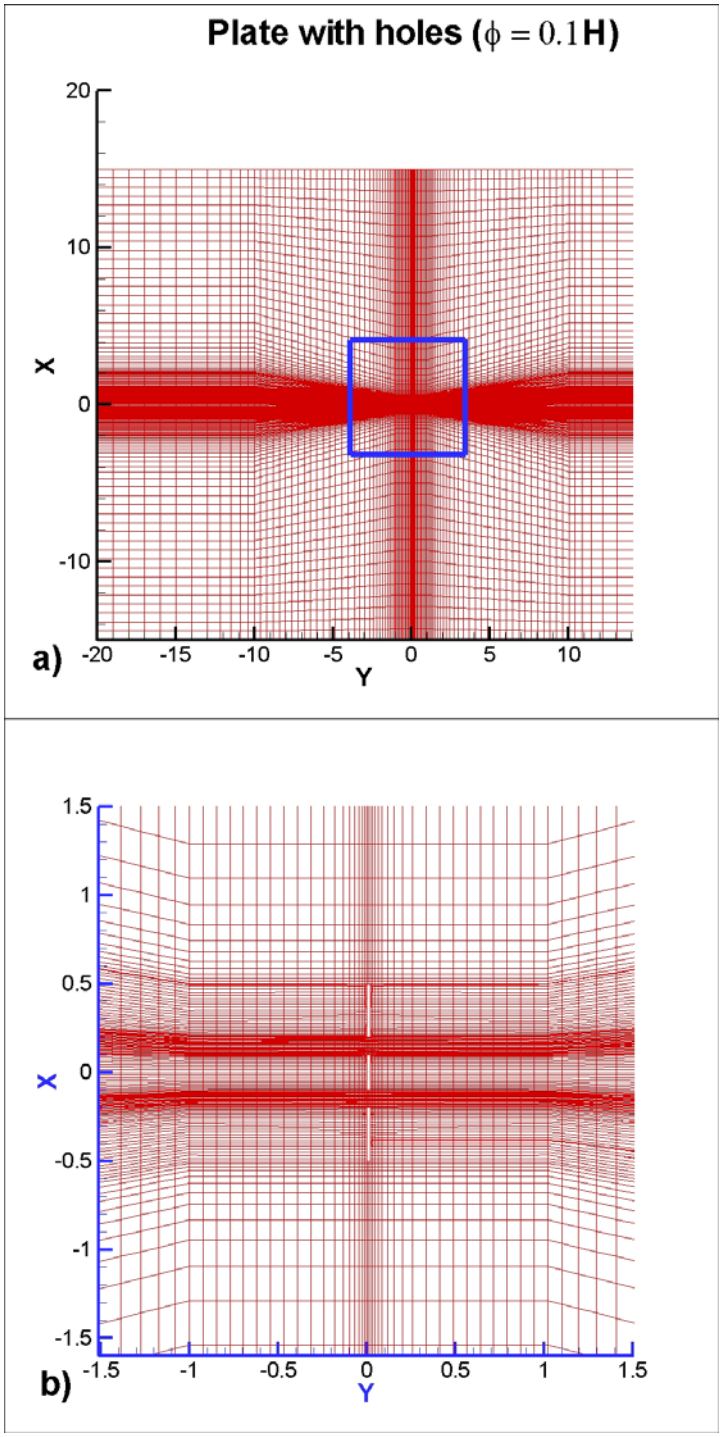

Figure 31. Visualization of the computational mesh for the panel with holes in a vertical plane cutting through the middle of the panel. a) general view, b) detail view of the mesh near the panel.

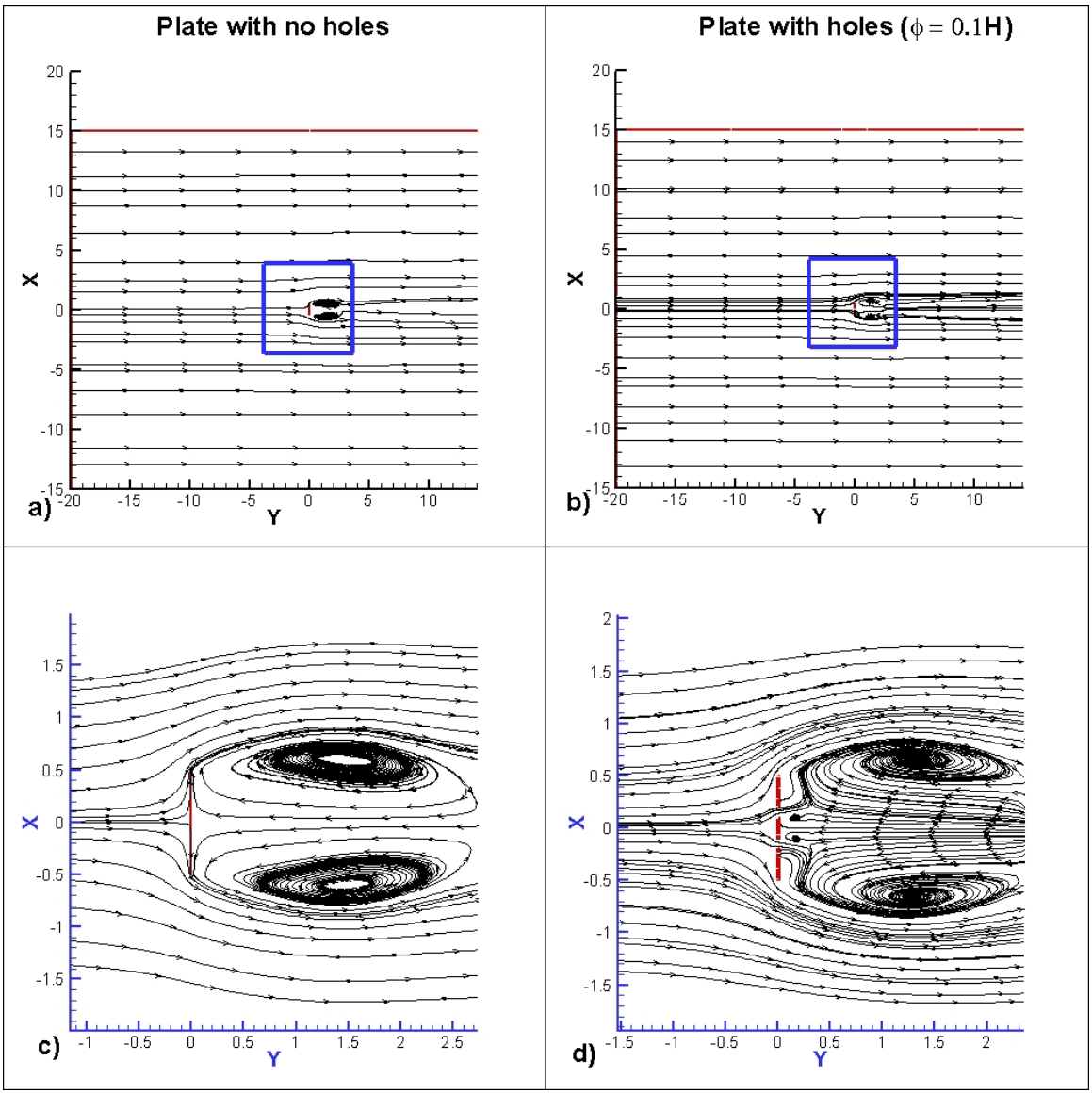

Figure 32. Streamlines in a vertical plane passing through the center of the panel. a) panel without holes, b) panel with holes, c) detail view, panel without holes, d) detail view, panel with holes.

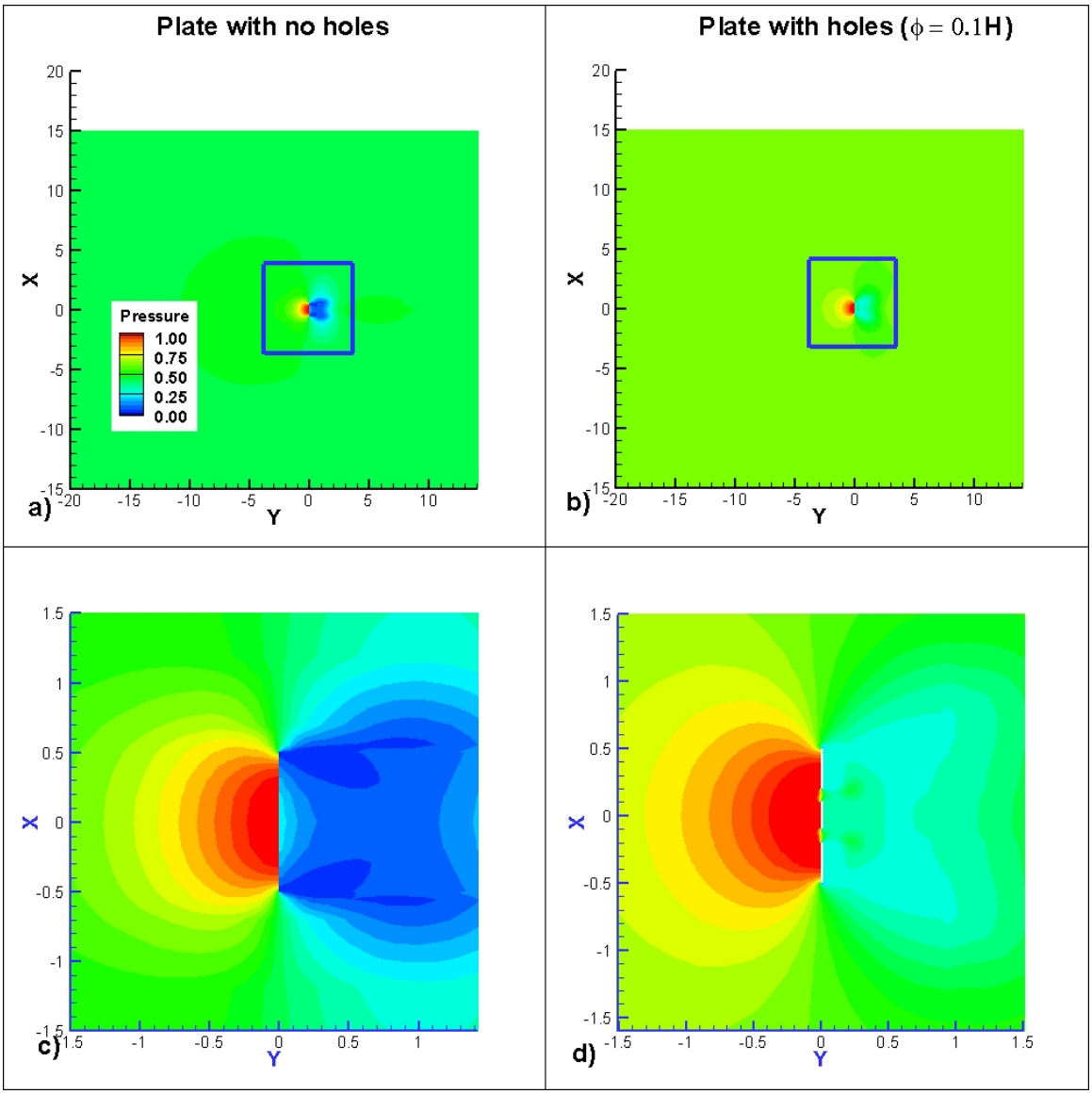

Figure 33. Pressure contours in a vertical plane passing through the center of the panel. a) panel without holes, b) panel with holes, c) detail view, panel without holes, d) detail view, panel with holes.

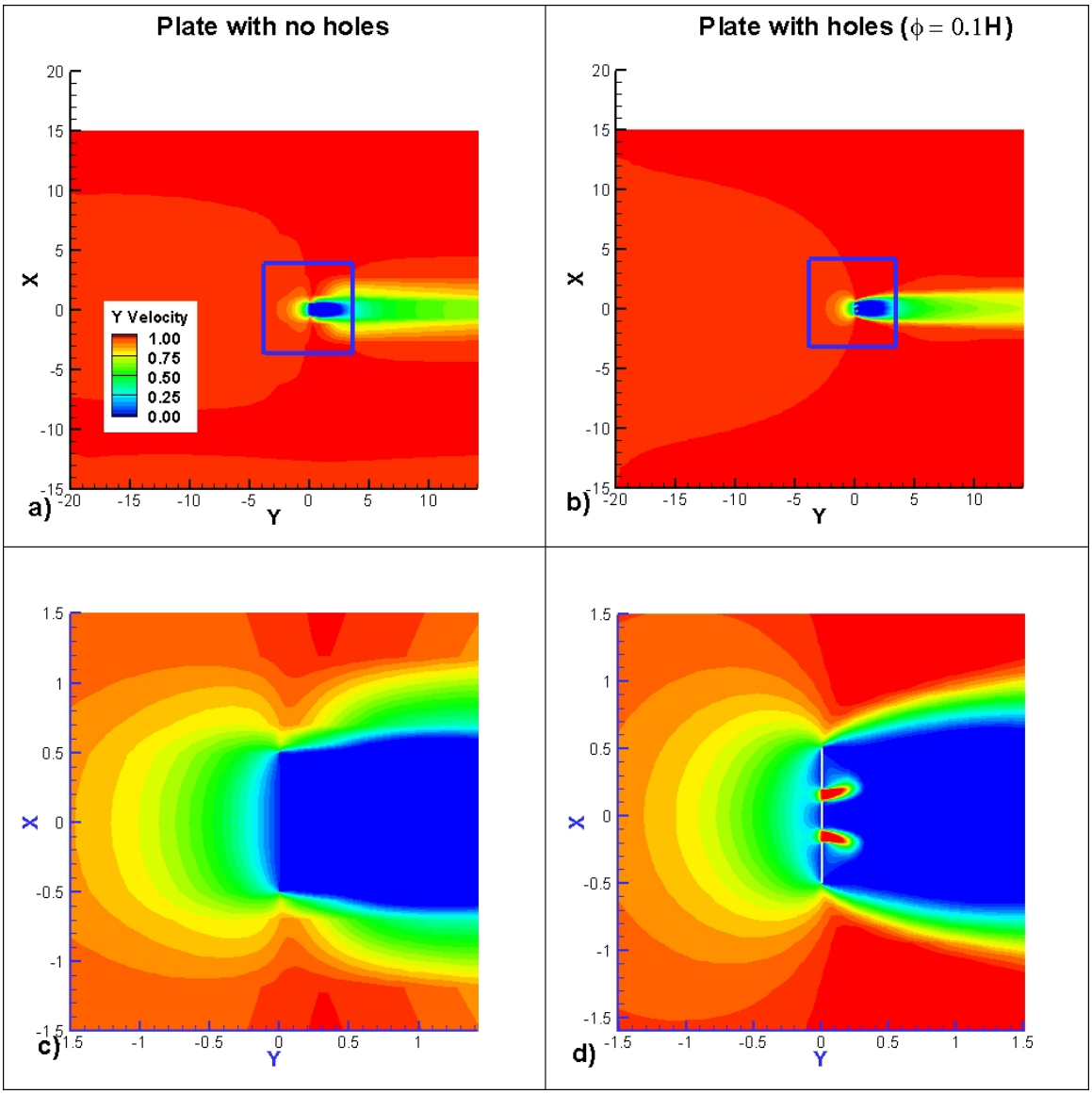

Figure 34. Streamwise velocity contours in a vertical plane passing through the center of the panel. a) panel without holes, b) panel with holes, c) detail view, panel without holes, d) detail view, panel with holes.

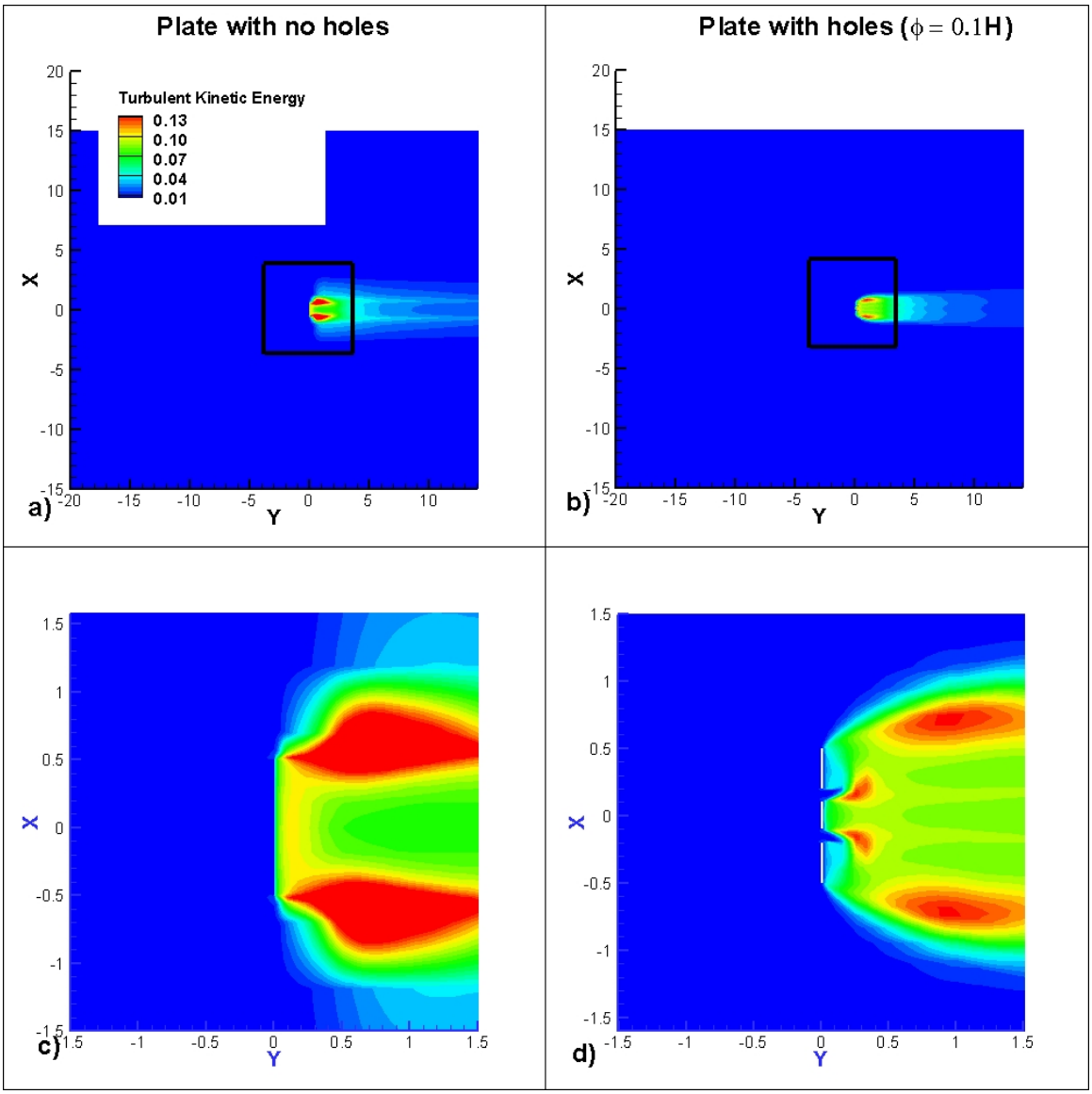

Figure 35. Turbulent kinetic energy (TKE) contours in a vertical plane passing through the center of the panel. a) panel without holes, b) panel with holes, c) detail view, panel without holes, d) detail view, panel with holes.

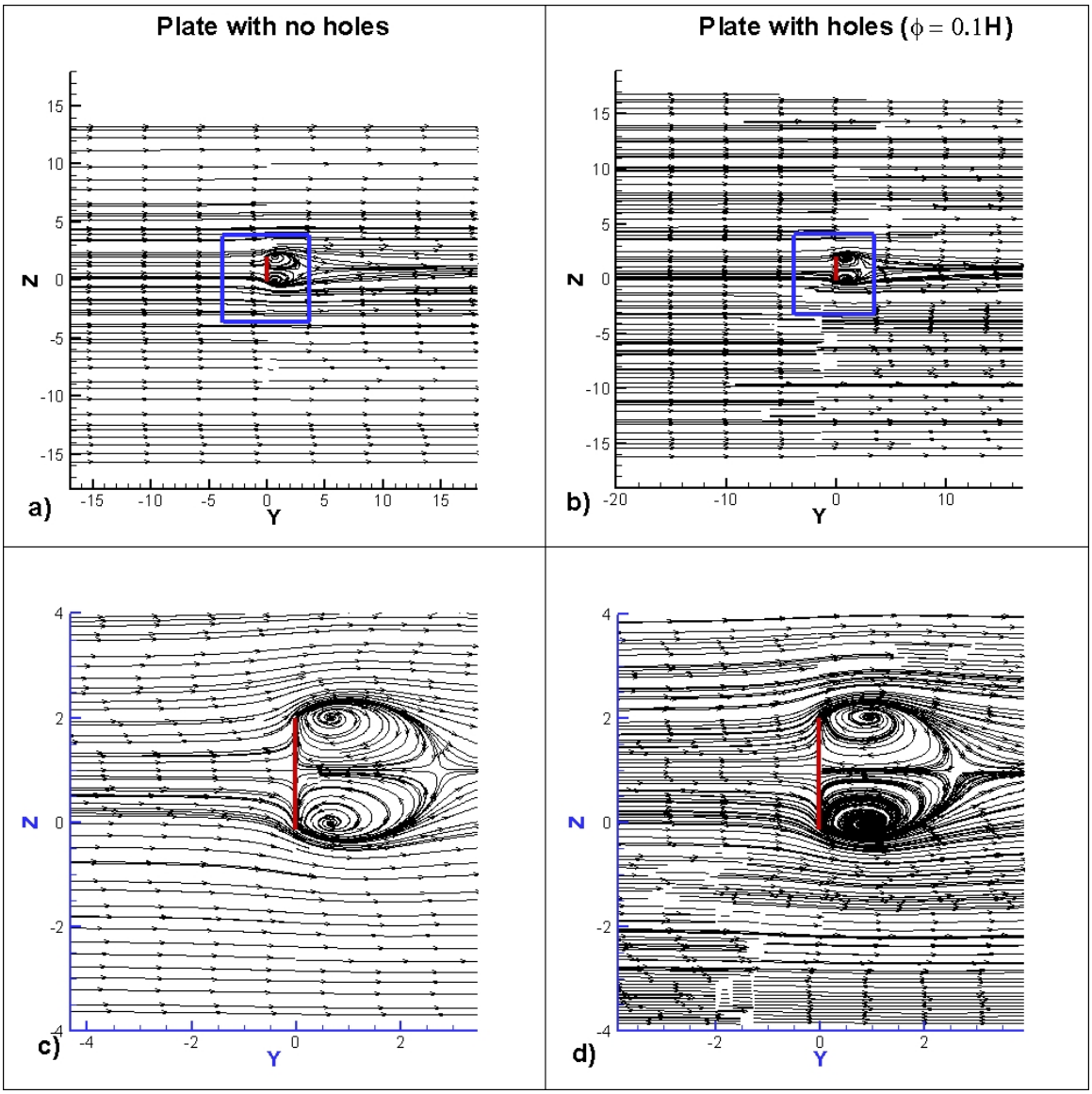

Figure 36. Streamlines in a horizontal plane passing through the center of the panel. a) panel without holes, b) panel with holes, c) detail view, panel without holes, d) detail view, panel with holes.

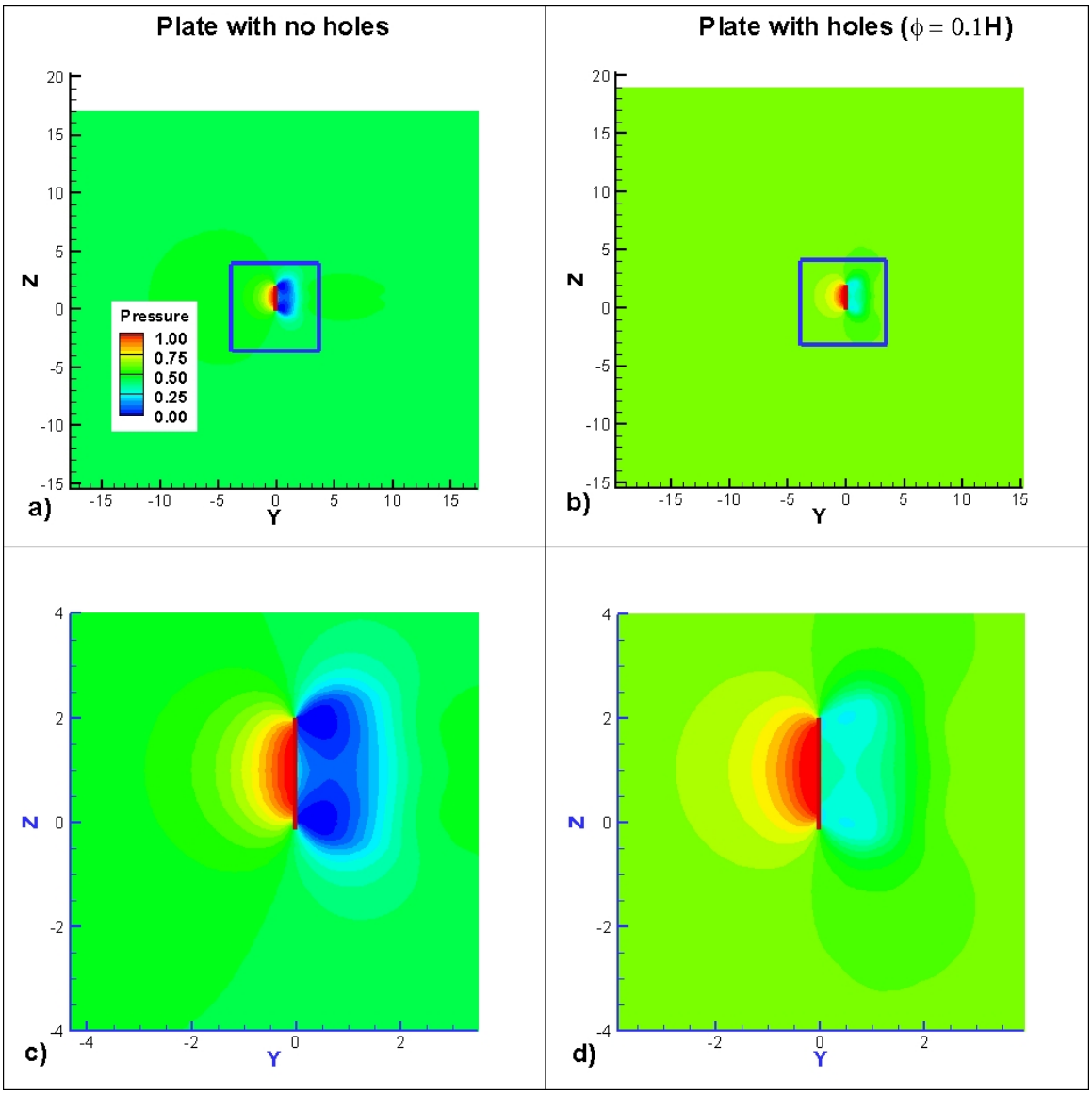

Figure 37. Pressure contours in a horizontal plane passing through the center of the panel. a) panel without holes, b) panel with holes, c) detail view, panel without holes, d) detail view, panel with holes.

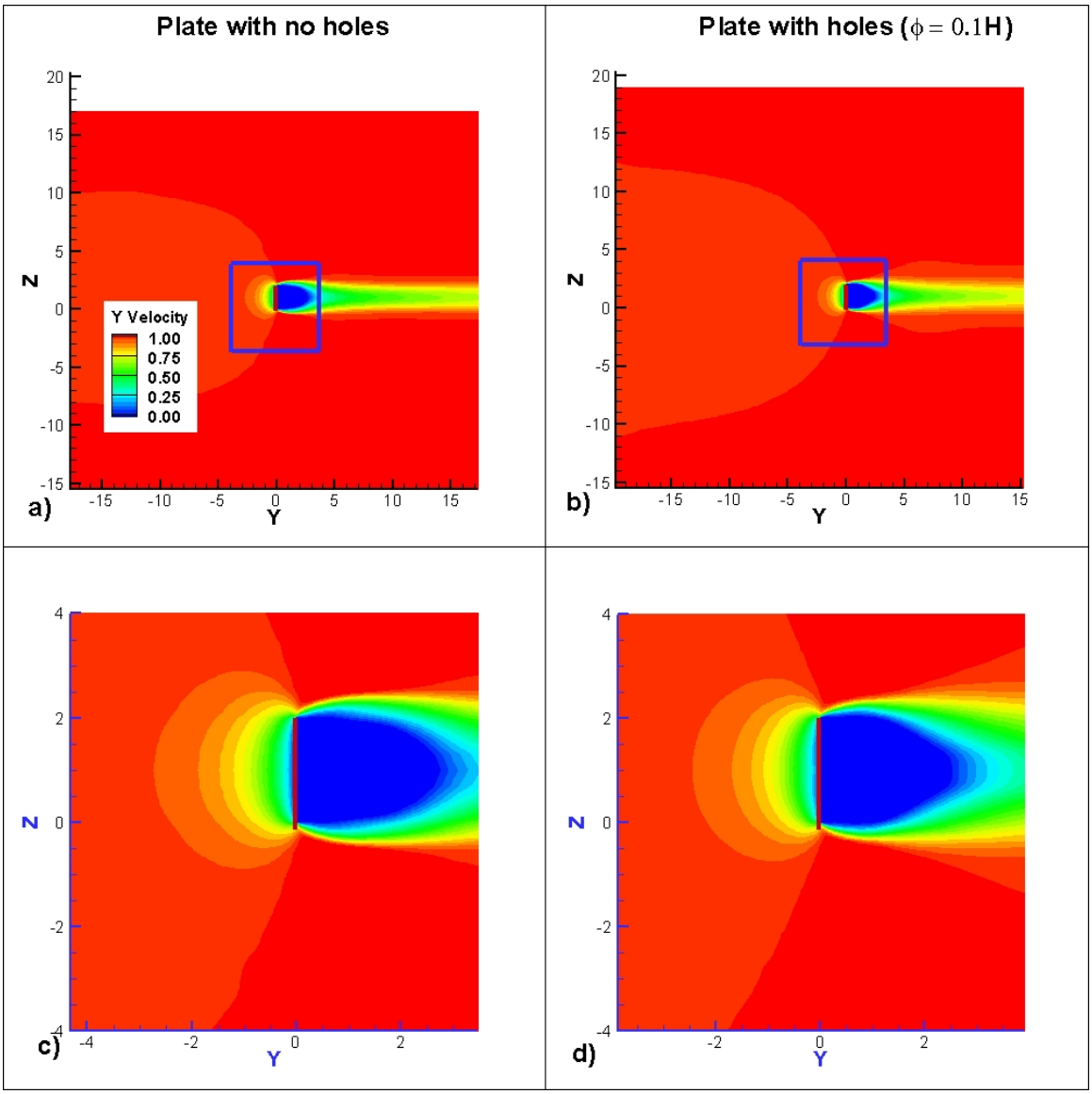

Figure 38. Streamwise velocity contours in a horizontal plane passing through the center of the panel. a) panel without holes, b) panel with holes, c) detail view, panel without holes, d) detail view, panel with holes.

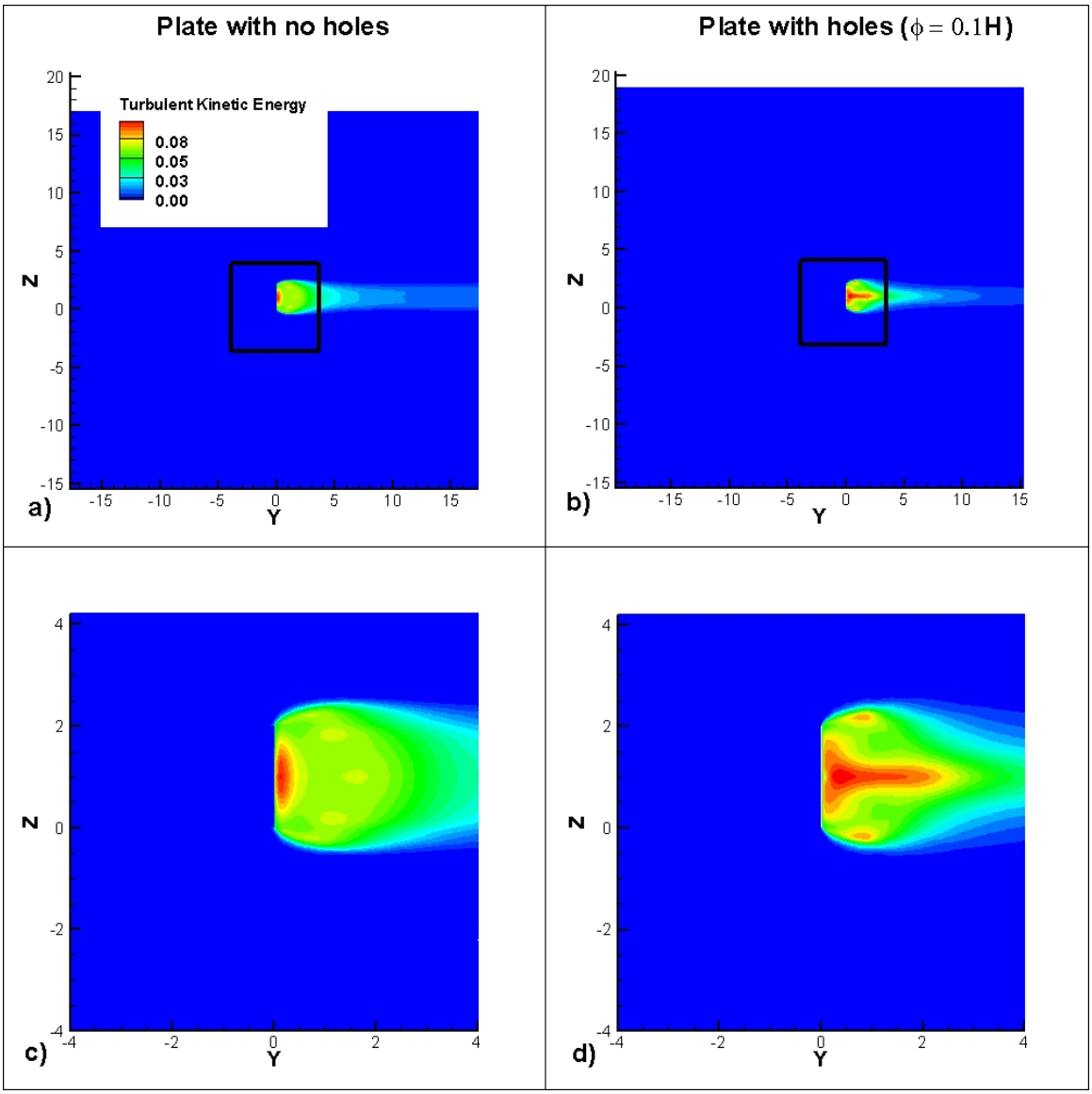

Figure 39. Turbulent kinetic energy contours in a plane passing through the center of the panel. a) panel without holes, b) panel with holes, c) detail view, panel without holes, d) detail view, panel with holes.